

Supporting Information:

Metalloporphycenes: Synthesis and
Characterization of
(Pentamethylcyclopentadienyl)ruthenium
Sitting-Atop and π -Complexes

*Luciano Cuesta,^a Elizabeth Karnas,^a Vincent M. Lynch,^a Ping Chen,^b Jing Shen,^b
Karl M. Kadish,^{*b} Kei Ohkubo,^c Shunichi Fukuzumi,^{*c} and Jonathan L. Sessler^{*a}*

^aDepartment of Chemistry & Biochemistry, University Station-A5300, The University of Texas, Austin, Texas 78712-0165, USA. ^bDepartment of Chemistry, University of Houston, Houston, Texas 77204-5003, USA. ^cDepartment of Material and Life Science, Graduate School of Engineering, Osaka University, SORST, Japan Science and Technology Agency (JST), Suita, Osaka 565-0871, Japan.

Contents	Page
Experimental Section: Instrumentation, Synthesis and Characterization of all New Compounds	5-11
Figure S1. ^1H and ^{13}C NMR in CDCl_3 and Mass Spectra for 1a .	12
Figure S2. UV-Vis absorption, emission (excitation at 560 nm) and excitation (emission at 670 nm) spectra of 1a recorded in PhCN.	13
Figure S3. Phosphorescence lifetime of 1a (excitation at 540 nm) recorded in PhCN at 298 K.	13
Figure S4. ^1H and ^{13}C NMR in CDCl_3 and Mass Spectra for 1b .	14
Figure S5. UV-Vis absorption, emission (excitation at 560 nm) and excitation (emission at 673 nm) spectra of 1b recorded in PhCN.	15
Figure S6. a) Transient absorption spectra of 1b in PhCN taken at the indicated times after femtosecond laser pulse irradiation by a 395 nm laser at 298 K. b) Decay time profile of the absorbance feature at 565 nm.	15
Figure S7. ^1H and ^{13}C NMR in CDCl_3 and Mass Spectra for 1c .	16
Figure S8. UV-Vis absorption, emission (excitation at 560 nm) and excitation (emission at 643 nm) spectra of 1c recorded in PhCN.	17
Figure S9. a) Transient absorption spectra of 1c in PhCN taken at the indicated times after femtosecond laser pulse irradiation by a 395 nm laser at 298 K. b) Decay time profile of the absorbance feature at 562 nm.	17
Figure S10. ^1H and ^{13}C NMR in CDCl_3 and Mass Spectra for 2a .	18
Figure S11. UV-Vis spectra of 2a and its ruthenium-free precursor, (EtiopC)Ni recorded in CH_2Cl_2 .	19
Figure S12. Decay time profile of the absorbance feature at 480 and at 1000 nm of 2a in CH_2Cl_2 (Corresponds to fs lfp shown in Figure 12b of article text). Both were best fit to a single exponential.	19
Figure S13. Decay time profile of the absorbance feature at 480 (single exponential) and at 640 nm (double exponential) for the ruthenium-free precursor to 2a in CH_2Cl_2 (Corresponds to fs lfp shown in Figure 12a of article text).	19
Figure S14. ^1H and ^{13}C NMR in CDCl_3 and Mass Spectra for 2b .	20
Figure S15. UV-Vis spectra of 2b and its ruthenium-free precursor (OEPc)Ni recorded in CH_2Cl_2 .	21

Figure S16. a) Transient absorption spectra of 2b in CH ₂ Cl ₂ taken at the indicated times after femtosecond laser pulse irradiation by a 420 nm laser at 298 K. b) Decay time profile of the absorbance feature at 480 and at 1000 nm. Both were best fit to a single exponential.	21
Figure S17. a) Transient absorption spectra of the ruthenium-free precursor to 2b , (OEPc)Ni in CH ₂ Cl ₂ taken at the indicated times after femtosecond laser pulse irradiation by a 390 nm laser at 298 K. b) Decay time profile of the absorbance feature at 480 (single exponential) and at 640 nm (double exponential decay).	21
Figure S18. ¹ H and ¹³ C NMR in CDCl ₃ and Mass Spectra for 2c .	22
Figure S19. UV-Vis spectra of 2c and its ruthenium-free precursor, (TPrPc)Ni recorded in CH ₂ Cl ₂ .	23
Figure S20. a) Transient absorption spectra of 2c in CH ₂ Cl ₂ taken at the indicated times after femtosecond laser pulse irradiation by a 420 nm laser at 298 K. b) Decay time profile of the absorbance feature at 480 and at 1000 nm. Both were fit to a single exponential.	23
Figure S21. a) Transient absorption spectra of the ruthenium-free precursor to 2c , (TPrPc)Ni in CH ₂ Cl ₂ taken at the indicated times after femtosecond laser pulse irradiation by a 390 nm laser at 298 K. b) Decay time profile of the absorbance feature at 480 (single exponential) and at 640 nm (double exponential decay).	23
Figure S22. Mass Spectrum of 3a .	24
Figure S23. ESR taken in CH ₂ Cl ₂ at 4 K (a) 3a , [(EtioPc)Cu(RuCp*)](PF ₆) (b) 3a , [(EtioPc)Cu(RuCp*)](PF ₆) after treating with one equiv. of Ru(bpy) ₃ ³⁺	24
Figure S24. UV-Vis spectra of 3a and the ruthenium-free precursor to 3a , (EtioPc)Cu recorded in CH ₂ Cl ₂ .	25
Figure S25. a) Transient absorption spectra of 3a in CH ₂ Cl ₂ taken at the indicated times after femtosecond laser pulse irradiation by a 420 nm laser at 298 K. b) Decay time profile of the absorbance feature at 500 nm (□) and at 1100 nm (■). Rates were determined by fit of a double exponential to the time profile at 500 nm.	25
Figure S26. Transient absorption spectra of the ruthenium-free precursor to 3a , (EtioPc)Cu in CH ₂ Cl ₂ taken at the indicated times after femtosecond laser pulse irradiation by a 390 nm laser at 298	25
Figure S27. Mass Spectrum for 3b .	26
Figure S28. UV-Vis spectra of 3b , and the ruthenium-free precursor to 3b , (OEPc)Cu recorded in CH ₂ Cl ₂ .	27

Figure S29. Transient absorption spectra of the ruthenium-free precursor to 3b , (OEPc)Cu in CH ₂ Cl ₂ taken at the indicated times after femtosecond laser pulse irradiation by a 390 nm laser at 298 K	27
Figure S30. Mass Spectrum for 3c .	28
Figure S31. ESR taken in CH ₂ Cl ₂ at 4 K (a) 3c , [(TPrPc)Cu(RuCp*)](PF ₆) (b) 3c , [(TPrPc)Cu(RuCp*)](PF ₆) after treating with one equiv. of Ru(bpy) ₃ ³⁺	28
Figure S32. UV-Vis spectra of 3c , and the ruthenium-free precursor to 3c , (TPrPc)Cu recorded in CH ₂ Cl ₂ .	29
Figure S33. a) Transient absorption spectra of 3c in CH ₂ Cl ₂ taken at the indicated times after femtosecond laser pulse irradiation by a 420 nm laser at 298 K. b) Decay time profile of the absorbance features at 480 (□)1000 (■) nm.	29
Figure S34. Transient absorption spectra of the ruthenium-free precursor to 3c , (TPrPc)Cu in CH ₂ Cl ₂ taken at the indicated times after femtosecond laser pulse irradiation by a 390 nm laser at 298 K	29
Figure S35. DFT calculations for 3a	30
Table S1. Half-wave Potentials (V vs SCE) of Ni and Cu Porphycenes	31
Figure S36. Cyclic voltammograms of (a) (EtioPc)RuCp*(PF ₆) (1a), (b) (OEPc)RuCp*(PF ₆) (1b), and (c) (TPrPc)RuCp*(PF ₆) (1c) under -70°C in CH ₂ Cl ₂ containing 0.1 M TBAPF ₆ .	32
Figure S37. Plot of (a) $E_{1/2}$ (V vs SCE, for [M ^{II} Pc]/[M ^I Pc]) vs metal electronegativity of porphycenes and (b) the lowest energy transition (λ_{\max} , cm ⁻¹ 10 ⁻³) vs radius of central metal ion.	33
Figure S38. Cyclic voltammograms of complexes 2-3 in CH ₂ Cl ₂ containing 0.1 M TBAPF ₆ .	34
Figure S39. UV-visible spectral changes of 2a and 2b during the first reduction in CH ₂ Cl ₂ , 0.1 M TBAPF ₆ .	35
Figure S40. UV-visible spectral changes of 3a , and 3b during the first reduction in CH ₂ Cl ₂ , 0.1 M TBAPF ₆ .	35
Calculation of the distance between the Two Unpaired Electrons as deduced from the Zero-Field Splitting Constants	36
SI references	36-37

Experimental Section

General Experimental Procedures. Prior to use, all glassware was soaked in KOH-saturated isopropyl alcohol for ca. 12 h and then rinsed with water and acetone before being thoroughly dried. Dichloromethane was freshly distilled from CaH_2 . *n*-Pentane was stirred over concentrated H_2SO_4 for more than 24h, neutralized with K_2CO_3 , and distilled from CaH_2 . Free-base porphycenes,^{S1} Ni(II) and Cu(II) metallo-porphycenes^{23,S2} were prepared following reported procedures. $[\text{Ru}(\text{Cp}^*)(\text{CH}_3\text{CN})_3][\text{PF}_6]$ was purchased commercially (Strem) and used as received. Solutions were stirred magnetically.

Nuclear magnetic resonance (NMR) spectra were obtained on a Varian Mercury 400 MHz. High-resolution mass spectra were obtained at the University of Texas at Austin, Department of Chemistry and Biochemistry, Mass Spectrometry Facility. Elemental analyses were performed by Midwest Microlabs Inc., Indianapolis, IN.

Cyclic voltammetry was carried out with an EG&G Princeton Applied Research (PAR) 173 potentiostat/galvanostat. A homemade three-electrode cell was used for cyclic voltammetric measurements and consisted of a glassy carbon working electrode, a platinum counter electrode, and a homemade saturated calomel reference electrode (SCE). UV-visible spectroelectrochemical experiments were performed with a homemade thin-layer cell that had a light transparent platinum net working electrode.^{S3} Potentials were applied and monitored with an EG&G PAR Model 173 potentiostat. Time-resolved UV-visible spectra were recorded with a Hewlett-Packard Model 8453 diode array spectrophotometer.

Femtosecond laser flash photolysis was conducted using a Clark-MXR 2010 laser system and an optical detection system provided by Ultrafast Systems (Helios). Typically, 5000 excitation pulses were averaged to obtain the transient spectrum at a set delay time. The kinetic traces at appropriate wavelengths were assembled from the time-resolved spectral data. Nanosecond time-resolved transient absorption measurements were carried out using the laser system provided by UNISOKU Co., Ltd. The photodynamics were monitored by continuous exposure to a xenon lamp (150 W) as a probe light and a photomultiplier tube (Hamamatsu 2949) as a detector. Transient spectra were recorded using fresh solutions in each laser excitation. The solution was deoxygenated by argon purging for 15 min prior to measurements.

EPR spectra were recorded on a JEOL JES-RE1XE spectrometer at 4K and 298 K. The magnitude of modulation was chosen to optimize the resolution and signal-to-noise (S/N) ratio of the observed spectra under non-saturating microwave power conditions. The g values were calibrated using an Mn^{2+} marker. The hyperfine coupling constants were determined by computer simulation using a Calleo ESR Version 1.2 program coded by Calleo Scientific on a personal computer.

Theoretical Calculations. Density-functional theory (DFT) calculations were performed on an 8CPU workstation (PQS, Quantum Cube QS8-2400C-064). Geometry optimization of **3a** was carried out using the Becke3LYP functional and Lan12dz basis set as implemented in the Gaussian 03 program Revision C.02. Graphical outputs of the computational results were generated with thse Gauss View software program (ver. 3.09) developed by Semichem, Inc.

General Synthesis of Compounds 1a-c: Excess $[\text{Ru}(\text{Cp}^*)(\text{CH}_3\text{CN})_3][\text{PF}_6]$ (45 mg, 0.09 mmol) was added to a solution of the respective free-base porphycene (0.03 mmol) in dry CH_2Cl_2 (30 mL) containing 5% of acetonitrile. The reaction mixture was heated at reflux under an argon atmosphere for 2 h, and the solvent was evaporated off. The crude product was purified by chromatography over alumina, eluting with $\text{MeOH}-\text{CH}_2\text{Cl}_2$ (0-5%). The second dark blue fraction was collected and the resulting product was recrystallized from $\text{CH}_2\text{Cl}_2/n$ -pentane.

Compound 1a: Yield (8 mg, 30%). ^1H NMR (400 MHz, 296 K, CDCl_3): δ (ppm) 9.72 (s, 4H, *meso*-H), 3.96 (q ($J = 7.5$ Hz), 8H, CH_2 - CH_3), 3.64 (s, 12H, Me), 1.72 (t ($J = 7.5$ Hz), 12H, CH_2 - CH_3), -1.17 (s, 15H, C_5Me_5). ^{13}C NMR (100.6 MHz, 296 K, CDCl_3): δ (ppm) 152.6, 149.2, 146.2, 131.8, 109.3, 106.5, 29.9, 20.9, 17.8, 16.3. HR-ESI (m/z): 713.3152 (calc. For $\text{C}_{42}\text{H}_{51}\text{N}_4\text{Ru}^{1+}$: 713.3157). Anal. Calcd. for $\text{C}_{42}\text{H}_{51}\text{N}_4\text{RuPF}_6$: C, 58.80; H, 5.99; N, 6.53. Found: C, 58.49; H, 6.27; N, 6.78.

Compound 1b: Yield (12 mg, 44%). ^1H NMR (400 MHz, 296 K, CDCl_3): δ (ppm) 9.75 (s, 4H, *meso*-H), 4.14–3.97 (m, 16H, CH_2 - CH_3), 1.78 (t ($J = 7.7$ Hz), 12H, CH_2 - CH_3), 1.60 (t ($J = 7.5$ Hz), 12H, CH_2 - CH_3), -1.16 (s, 15H, C_5Me_5). ^{13}C NMR (100.6 MHz, 296 K, CDCl_3): δ (ppm) 152.4, 148.9, 145.2, 138.8, 109.4, 106.5, 21.0, 20.8, 18.9, 18.5, 6.31. HR-ESI (m/z): 771.3934 (calc. For $\text{C}_{46}\text{H}_{61}\text{N}_4\text{Ru}^{1+}$ (M+2H): 771.3924). Anal. Calcd. for $\text{C}_{46}\text{H}_{59}\text{N}_4\text{RuPF}_6$: C, 60.45; H, 6.51; N, 6.13. Found: C, 60.09; H, 6.67; N, 6.08.

Compound 1c: Yield (9 mg, 34%). ^1H NMR (400 MHz, 296 K, CDCl_3): δ (ppm) 9.84 (s, 4H, *meso*-H), 9.01 (s, 4H, β -H), 4.09–3.97 (m, 8H, CH_2 - CH_2 - CH_3), 2.04–2.19 (m, 8H, CH_2 - CH_2 - CH_3), 1.25 (m, 12H, CH_2 - CH_2 - CH_3), -1.18 (s, 15H, C_5Me_5). ^{13}C NMR (100.6 MHz, 296 K, CDCl_3): δ (ppm) 154.1, 150.7, 145.2, 121.9, 110.5, 106.7,

31.7, 29.9, 25.3, 14.6. HR-ESI (m/z): 715.3308 (calc. For $C_{42}H_{53}N_4Ru^{1+}$ (M+2H): 715.3317 Anal. Calcd. for $C_{42}H_{51}N_4RuPF_6$: C, 58.80; H, 5.99; N, 6.53. Found: C, 58.99; H, 6.07; N, 6.18.

General Synthesis of Compounds 2a-c: A slight excess of $[Ru(Cp^*)(CH_3CN)_3][PF_6]$ (20 mg, 0.04 mmol) was added to a solution of the corresponding Ni(II)-porphycene (0.03 mmol) in dry CH_2Cl_2 (30 mL). The reaction mixture was heated at reflux for 1 h under argon atmosphere. The solvent was then evaporated off until a volume of ca. 2 mL remained. The resulting solution was then purified by means of thin layer chromatography over alumina, using MeOH- CH_2Cl_2 (1%) as the elute. The green-brownish band was stripped from the support using CH_2Cl_2 , and the resulting product was recrystallized from CH_2Cl_2/n -pentane.

Compound 2a: Yield (20 mg, 74%). 1H NMR (400 MHz, 296 K, $CDCl_3$): δ (ppm) 8.37, 8.31 (ABq ($J = 12.5$ Hz), 2H, *meso*-H), 8.26 (d ($J = 11.3$ Hz), 1H, *meso*-H), 7.74 (d ($J = 11.3$ Hz), 1H, *meso*-H) 3.27–3.12 (m, 6H, CH_2 - CH_3), 3.10 (q ($J = 7.9$ Hz), 2H, CH_2 - CH_3), 2.98 (s, 3H, Me), 2.92 (s, 3H, Me), 2.88 (s, 3H, Me), 2.85 (s, 3H, Me), 1.45–1.41 (m, 12H, CH_2 - CH_3), 0.88 (s, 15H, C_5Me_5). ^{13}C NMR (100.6 MHz, 296 K, $CDCl_3$): δ (ppm) 155.1, 154.8, 149.9, 145.7, 144.3, 129.7, 129.3, 126.0, 120.2, 119.5, 110.9, 106.7, 105.3, 103.2, 102.5, 99.8, 92.3, 91.9, 88.9, 87.0, 86.5, 38.8, 30.4, 29.9, 29.0, 23.8, 23.1, 19.8, 19.3, 14.3, 13.7, 13.0, 10.1, 9.3. HR-ESI (m/z): 771.2505 (calc. For $C_{42}H_{51}N_4NiRu^{1+}$: 771.2500). Anal. Calcd. for $C_{43}H_{53}N_4Cl_2NiRuPF_6$ (**2a**- CH_2Cl_2): C, 51.57; H, 5.33; N, 5.59. Found: C, 51.66; H, 5.47; N, 5.45.

Compound 2b: Yield (18 mg, 62%). 1H NMR (400 MHz, 296 K, $CDCl_3$): δ (ppm) 8.32–8.23 (m, 3H, *meso*-H), 7.81 (d ($J = 11.0$ Hz), 1H, *meso*-H), 3.34–3.14 (m, 12H,

CH_2-CH_3), 3.06 (q ($J = 7.2$ Hz), 2H, CH_2-CH_3), 2.89 (q ($J = 7.2$ Hz), 2H, CH_2-CH_3), 1.52-1.34 (m, 24H, CH_2-CH_3), 0.92 (s, 15H, C_5Me_5). ^{13}C NMR (100.6 MHz, 296 K, $CDCl_3$): δ (ppm) 155.8, 155.6, 155.0, 154.5, 154.4, 152.8, 147.9, 144.6, 141.9, 141.5, 139.8, 132.9, 120.7, 120.5, 111.1, 106.1, 105.5, 103.5, 102.5, 97.82, 86.9, 29.9, 20.4, 20.1, 19.7, 19.6, 19.5, 19.4, 18.4, 18.2, 18.1, 18.0, 17.5, 17.3, 17.2, 17.1, 16.9, 9.5. HR-ESI (m/z): 827.3131 (calc. For $C_{46}H_{59}N_4NiRu^{1+}$: 827.3121). Anal. Calcd. for $C_{46}H_{59}N_4NiRuPF_6$: C, 56.80; H, 6.11; N, 5.76. Found: C, 56.49; H, 6.07; N, 5.58.

Compound 2c: Yield (19 mg, 71%). 1H NMR (400 MHz, 296 K, $CDCl_3$): δ (ppm) 8.09–7.91 (m, 3H, 3 *meso*-H + 1 β -H), 7.74 (s, 1H, β -H), 7.68 (s, 1H, β -H), 7.57 (d ($J = 10.7$ Hz), 1H, *meso*-H), 6.61 (s, 1H, β -H), 3.30–2.92 (m, 8H, $CH_2-CH_2-CH_3$), 2.04–1.93 (m, 8H, $CH_2-CH_2-CH_3$), 1.34–1.16 (m, 12H, $CH_2-CH_2-CH_3$), 0.88 (s, 15H, C_5Me_5). ^{13}C NMR (100.6 MHz, 296 K, $CDCl_3$): δ (ppm) 158.8, 158.1, 157.9, 153.6, 152.9, 150.3, 147.9, 140.4, 137.8, 129.1, 123.1, 122.7, 121.5, 119.4, 118.7, 107.7, 105.8, 103.6, 101.4, 100.8, 88.7, 31.3, 30.5, 29.9, 28.5, 24.9, 24.5, 23.4, 23.3, 14.7, 14.5, 14.4, 14.3, 9.2. HR-ESI (m/z): 771.2505 (calc. For $C_{42}H_{51}N_4NiRu^{1+}$: 771.2517). Anal. Calcd. for $C_{42}H_{51}N_4NiRuPF_6$: C, 55.04; H, 5.61; N, 6.11. Found: C, 55.09; H, 5.47; N, 6.47.

General Synthesis of Compounds 3a-c: The corresponding Cu(II)-porphycene (0.03 mmol) and $[Ru(Cp^*)(CH_3CN)_3][PF_6]$ (20 mg, 0.04 mmol) precursors were heated at reflux in dry CH_2Cl_2 (30 mL) for 1 h under an argon atmosphere. The mixture was concentrated to a volume of ca. 2 mL, and the product was isolated by thin layer chromatography (alumina, 1% MeOH- CH_2Cl_2 , dark green band stripped off using CH_2Cl_2), followed by recrystallization from CH_2Cl_2/n -pentane.

Compound 3a: Yield (22 mg, 81%). HR-ESI (m/z): 776.2448 (calc. For $C_{42}H_{51}N_4CuRu^{1+}$: 776.2450). Anal. Calcd. for $C_{42}H_{51}N_4CuRuPF_6$: C, 54.75; H, 5.58; N, 6.08. Found: C, 54.69; H, 5.32; N, 6.15.

Compound 3b: Yield (20 mg, 69%). HR-ESI (m/z): 832.3074 (calc. For $C_{46}H_{59}N_4CuRu^{1+}$: 832.3086). Anal. Calcd. for $C_{46}H_{59}N_4CuRuPF_6$: C, 56.52; H, 6.08; N, 5.73. Found: C, 56.48; H, 6.37; N, 5.91.

Compound 3c: Yield (22 mg, 82%). HR-ESI (m/z): 776.2448 (calc. For $C_{42}H_{51}N_4NiRu^{1+}$: 776.2450). Anal. Calcd. for $C_{42}H_{51}N_4CuRuPF_6$: C, 54.75; H, 5.58; N, 6.08. Found: C, 54.79; H, 5.82; N, 6.37.

Crystal Structure Determinations for Complexes 1b, 1c, 2a, 3a. The data were collected on a Nonius Kappa CCD diffractometer using a graphite monochromator with $MoK\alpha$ radiation ($\lambda = 0.71073 \text{ \AA}$). Data collections were conducted at 153 K using an Oxford Cryostream low temperature device. Data reductions were performed using DENZO-SMN.^{S4} The structures were solved by direct methods using SIR97^{S5} and refined by full-matrix least-squares on F^2 with anisotropic displacement parameters for the non-H atoms using SHELXL-97.^{S6}

The following definitions apply to all the refinements:

$$R = \Sigma(|F_0| - |F_c|)/\Sigma|F_0| \text{ for reflections with } F_0 > 4(\Sigma(F_0)),$$

$$R_w = \{\Sigma w(|F_0|^2 - |F_c|^2)^2/\Sigma w|F_0|^4\}^{1/2}, \text{ where } w \text{ is the weight given each reflection.}$$

Goodness of fit, $S = [\Sigma w(|F_0|^2 - |F_c|^2)^2/(n - p)]^{1/2}$, where n is the number of reflections and p is the number of refined parameters. Unless otherwise specified, hydrogen atoms were calculated in ideal positions with isotropic displacement parameters set to $1.2 \times U_{eq}$ of the attached atom ($1.5 \times U_{eq}$ for methyl hydrogen atoms). Neutral

atom scattering factors and values used to calculate the linear absorption coefficients are from the International Tables for X-ray Crystallography.

In the case of **1c**, the crystal was twinned. The twin law was determined using ROTAX^{S7} to be (1,0,0/0,-1,0/0,0,-1) about 100 reciprocal lattice direction. The twin fraction refined to 0.260(5). ROTAX was used as incorporated in WinGX.^{S8} Severely overlapped reflections were omitted during refinement.

Crystal Data and Structure Refinement Parameters for Complexes **1b**, **1c**, **2a** and **3a**

	1b	1c	2a	3a
empirical formula	C ₄₆ H ₅₉ F ₆ N ₄	C ₄₂ H ₅₁ F ₆ N ₄	C ₄₂ H ₅₃ F ₆ Cl ₂ N ₄ N	C ₄₂ H ₅₃ F ₆ Cl ₂ N ₄ N
crystal	914.01	857.91	1001.54	1006.37
space group	monoclinic	monoclinic	triclinic	triclinic
a, Å	P21/c	P21/c	P-1	P-1
b, Å	12.3036(6)	21.737(2)	10.2140(2)	10.2466(7)
c, Å	29.362(2)	25.642(2)	12.5870(3)	12.5796(10)
α, °	11.8233(7)	13.8213(1)	17.5420(4)	17.5498(15)
β, °	90	90	73.766(1)	73.990(3)
γ, °	93.983(2)	90.525(5)	78.165(1)	77.861(3)
V, Å ³	90	90	82.810(1)	82.878(3)
Z	4260.9(4)	7703.4(11)	2113.78(8)	2120.5(3)
D (Calc'd), abs. coeff.,	4	8	2	2
F(000)	1.425	1.479	1.574	1.576
θ for data limiting	0.470	0.514	1.030	1.085
	1904	3552	1028	1030
	2.70 –	2.92 –	2.04 – 27.49	1.81 – 27.50
	-15 ≤ h ≤	-24 ≤ h ≤	-13 ≤ h ≤ 13	-13 ≤ h ≤ 11
	-38 ≤ k ≤	-30 ≤ k ≤	-16 ≤ k ≤ 15	-16 ≤ h ≤ 14
	-15 ≤ l ≤	-16 ≤ l ≤	-22 ≤ l ≤ 21	-22 ≤ h ≤ 21
Reflections collected	17779	11835	32634	14990
independent reflections	9642	11835	9632	9552
absorption correction	Semi-empirical from equivalents	Semi-empirical from equivalents	Ful-matrix least-squares on F ²	Semi-empirical from equivalents
data/restraint	9642/0/53	11835/648	9632/7/546	9552/64/548
goodness-of- R, R _w	1.121	1.232	1.087	1.029
	0.0619,	0.1020,	0.0545, 0.1103	0.0565, 0.1178

Compound 1a:

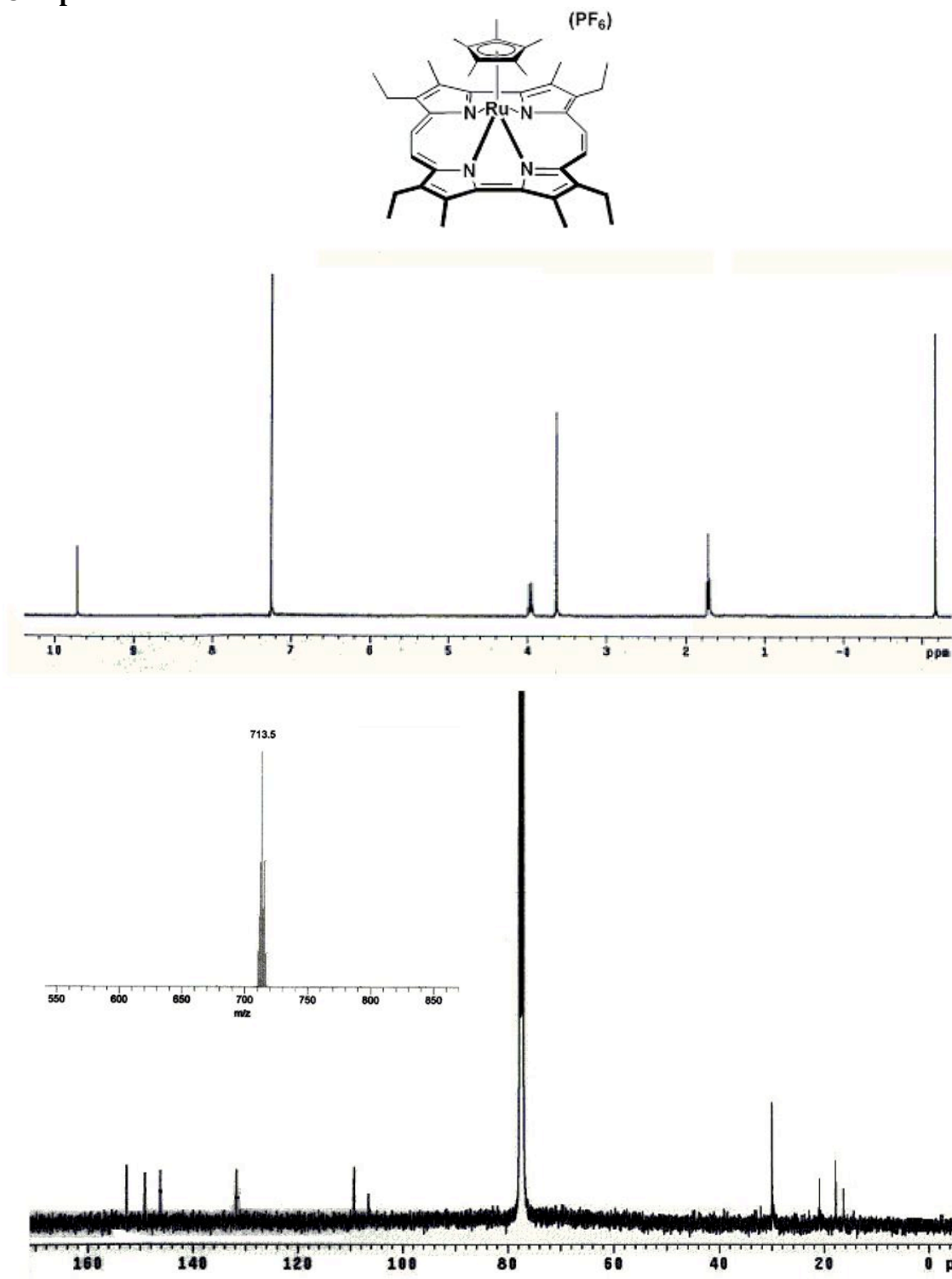


Figure S1. ¹H and ¹³C NMR in CDCl₃ and Mass Spectra for 1a.

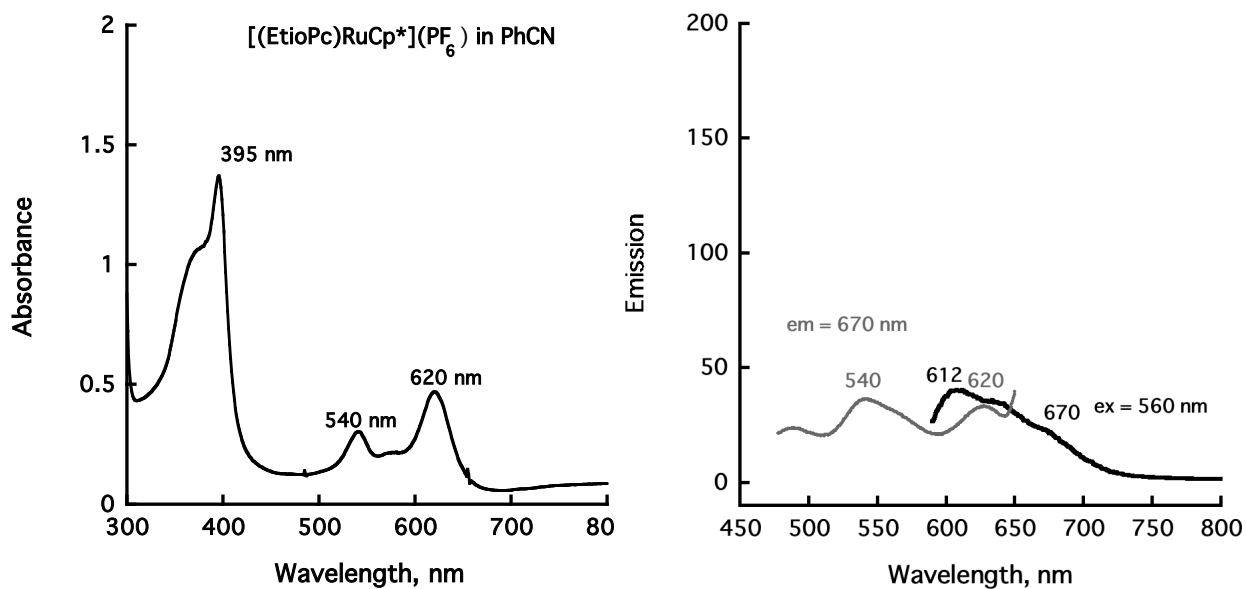


Figure S2. UV-Vis absorption, emission (excitation at 560 nm) and excitation (emission at 670 nm) spectra of **1a** recorded in PhCN.

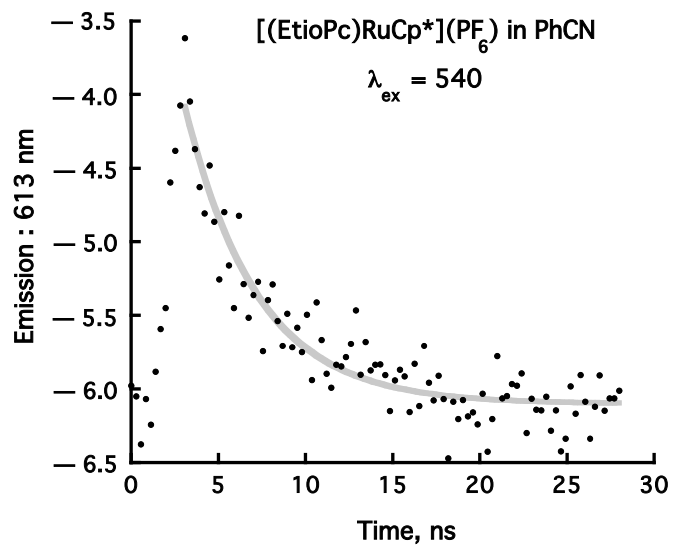


Figure S3. Phosphorescence lifetime of **1a** (excitation at 540 nm) recorded in PhCN at 298 K.

Compound 1b:

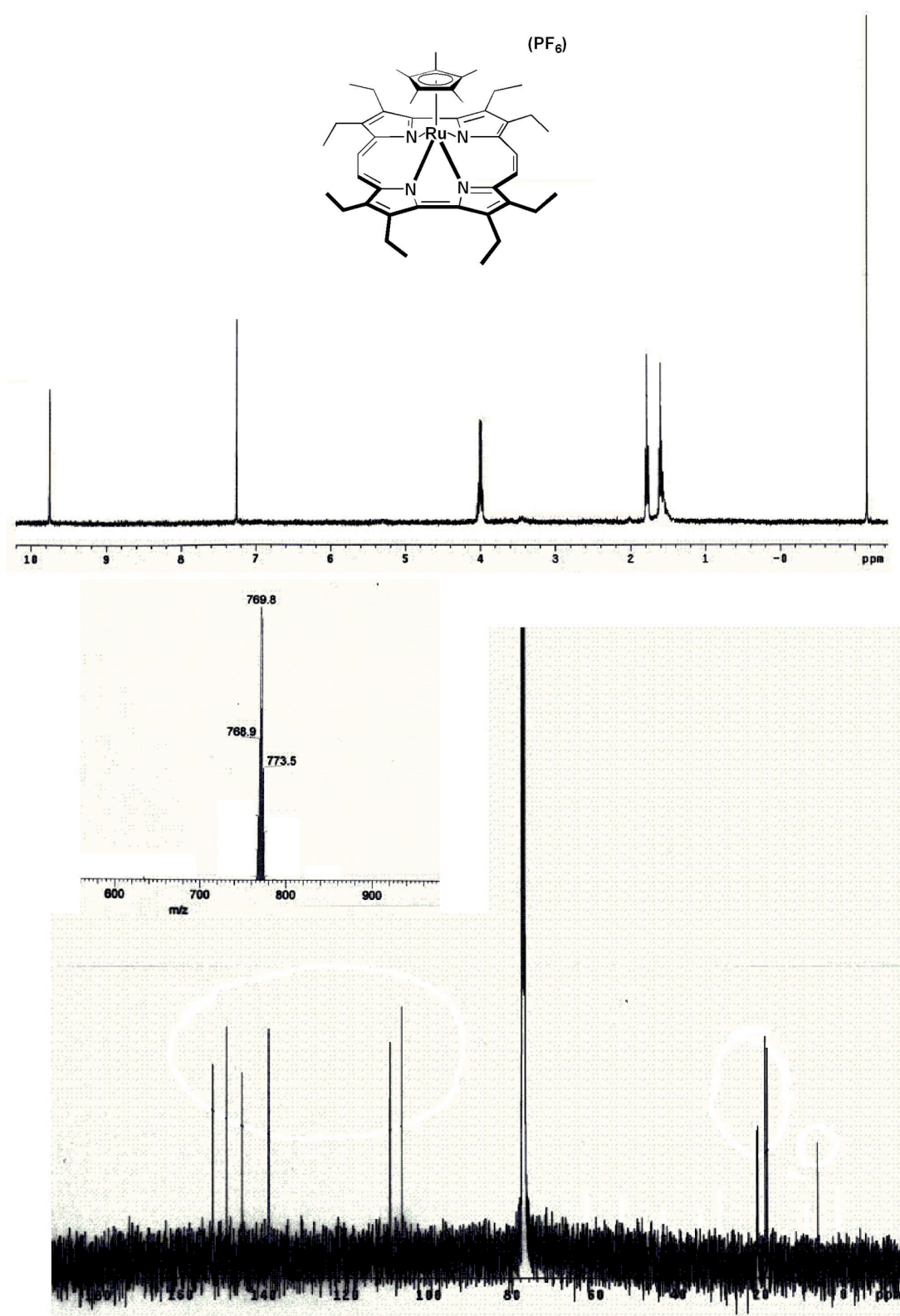


Figure S4. ¹H and ¹³C NMR in CDCl₃ and Mass Spectra for **1b**.

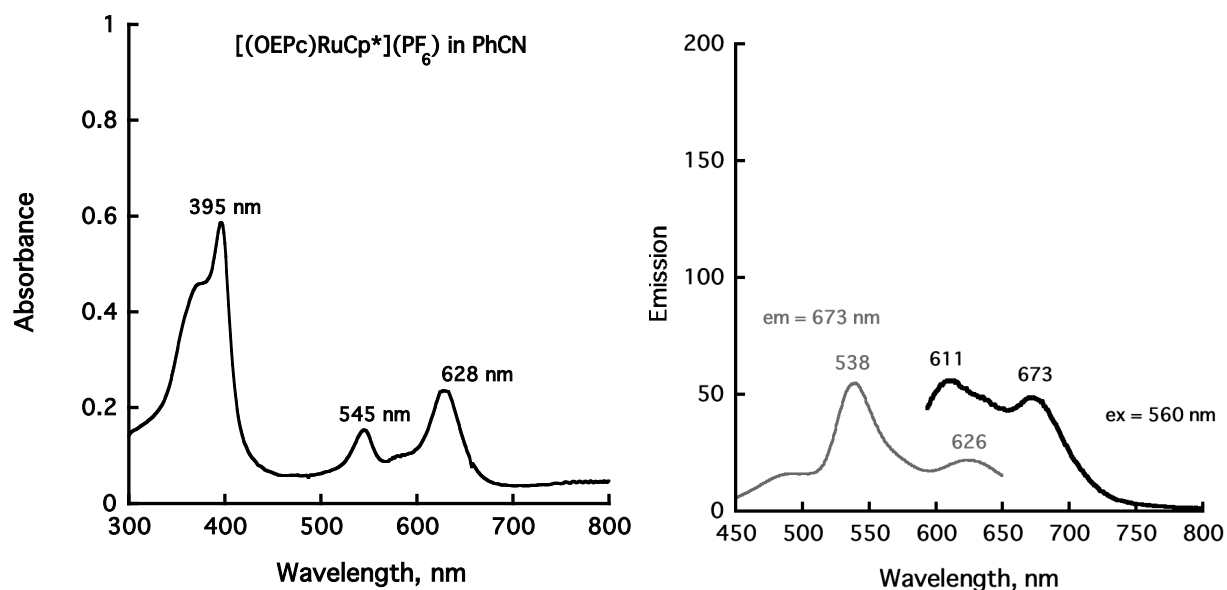


Figure S5. UV-Vis absorption, emission (excitation at 560 nm) and excitation (emission at 673 nm) spectra of **1b** recorded in PhCN.

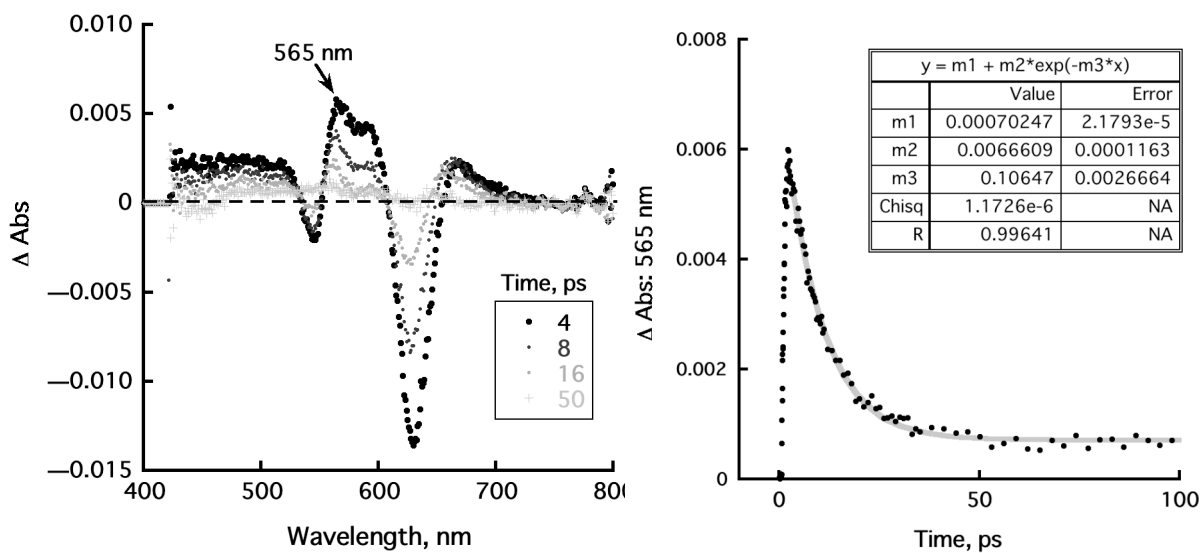


Figure S6. a) Transient absorption spectra of **1b** in PhCN taken at the indicated times after femtosecond laser pulse irradiation by a 395 nm laser at 298 K. b) Decay time profile of the absorbance feature at 565 nm.

Compound 1c:

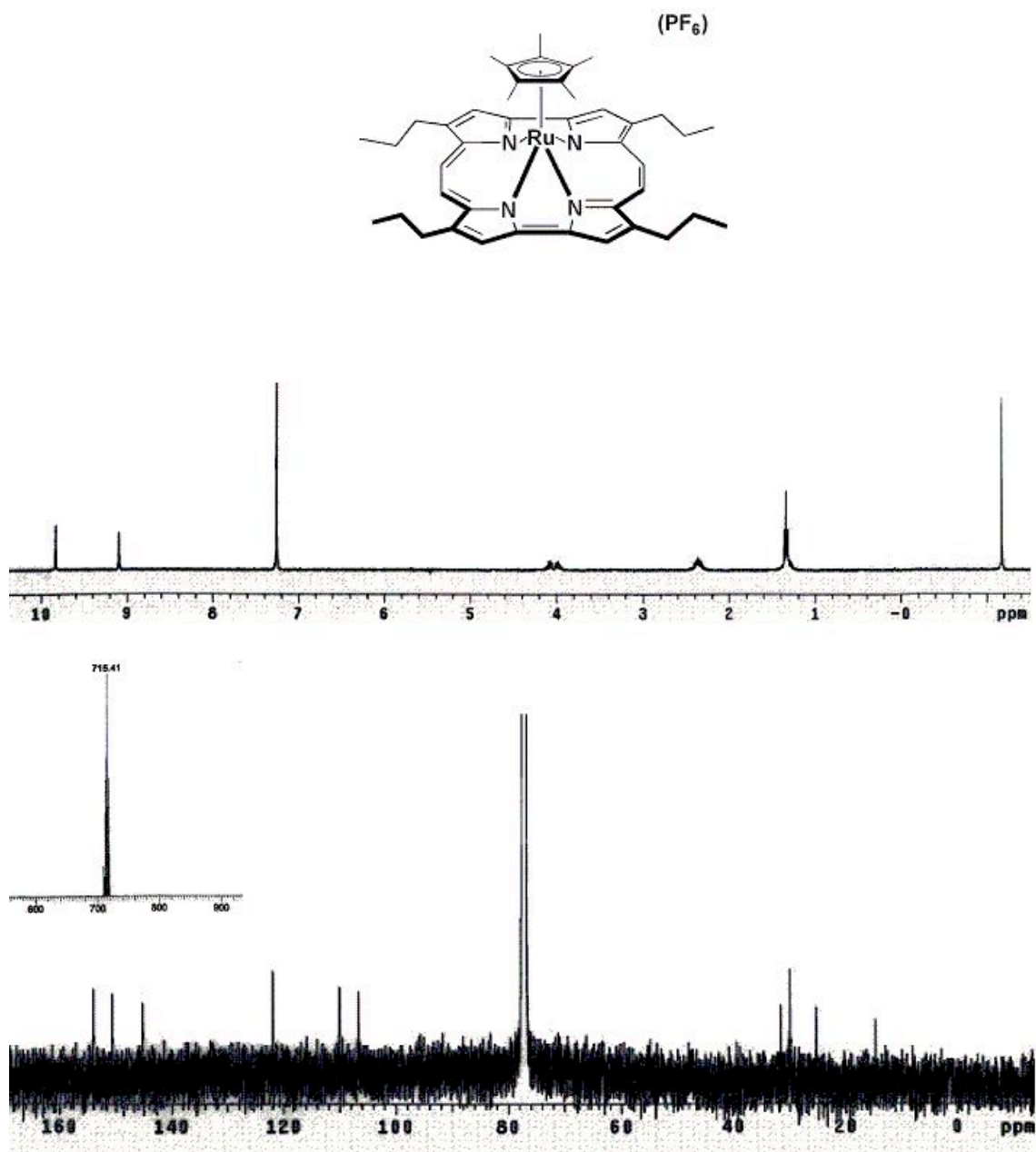


Figure S7. ¹H and ¹³C NMR in CDCl₃ and Mass Spectra for **1c**.

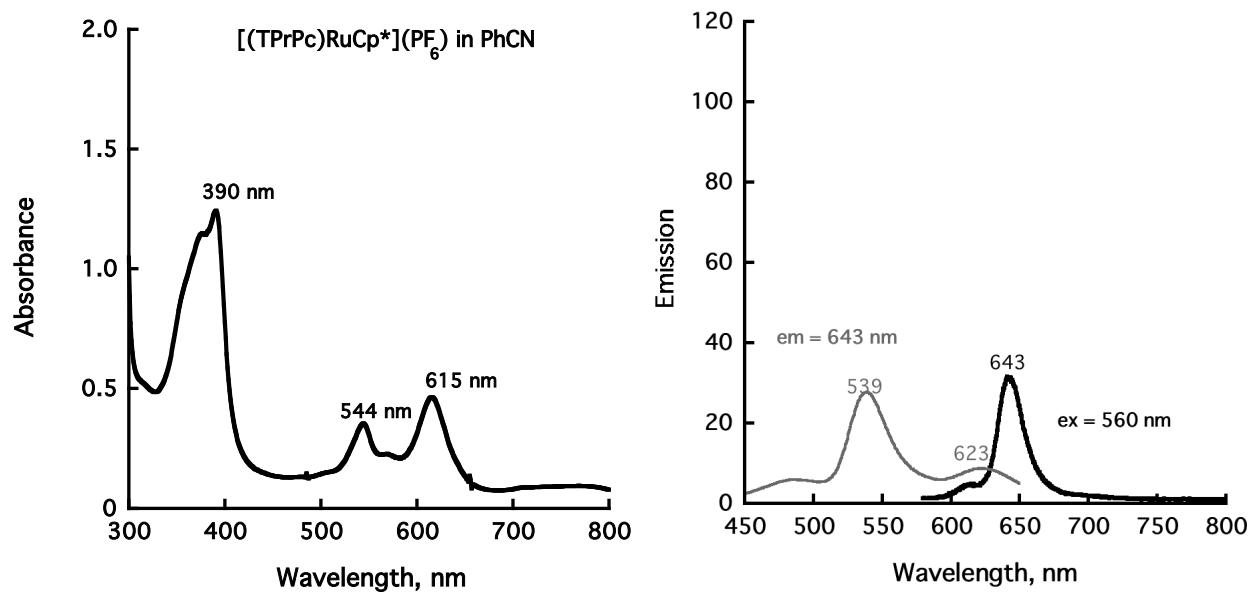


Figure S8. UV-Vis absorption, emission (excitation at 560 nm) and excitation (emission at 643 nm) spectra of **1c** recorded in PhCN.

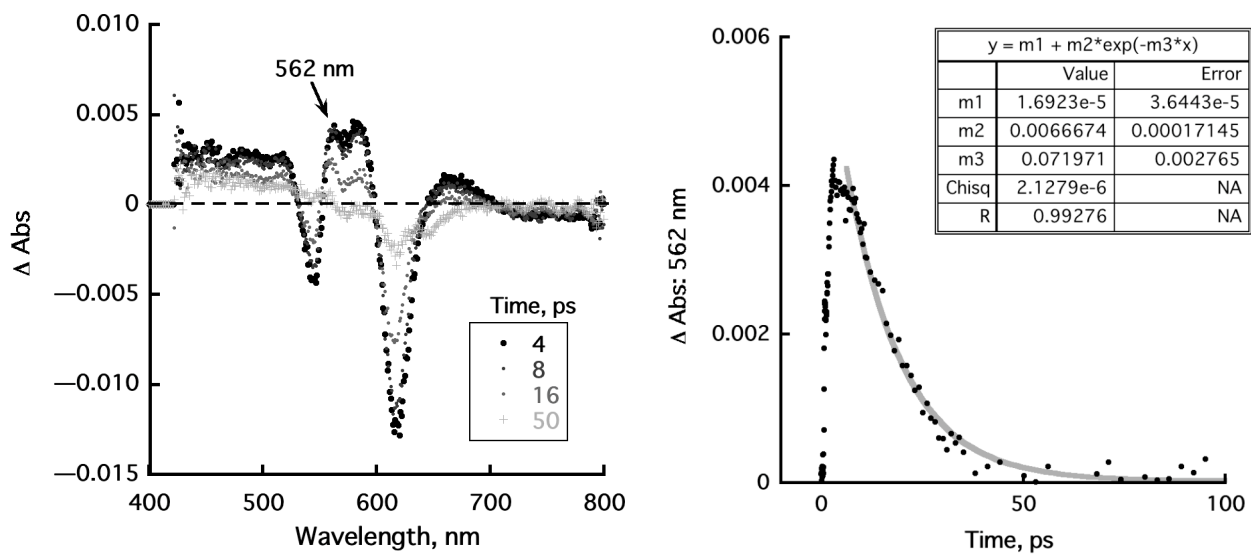


Figure S9. a) Transient absorption spectra of **1c** in PhCN taken at the indicated times after femtosecond laser pulse irradiation by a 395 nm laser at 298 K. b) Decay time profile of the absorbance feature at 562 nm.

Compound 2a:

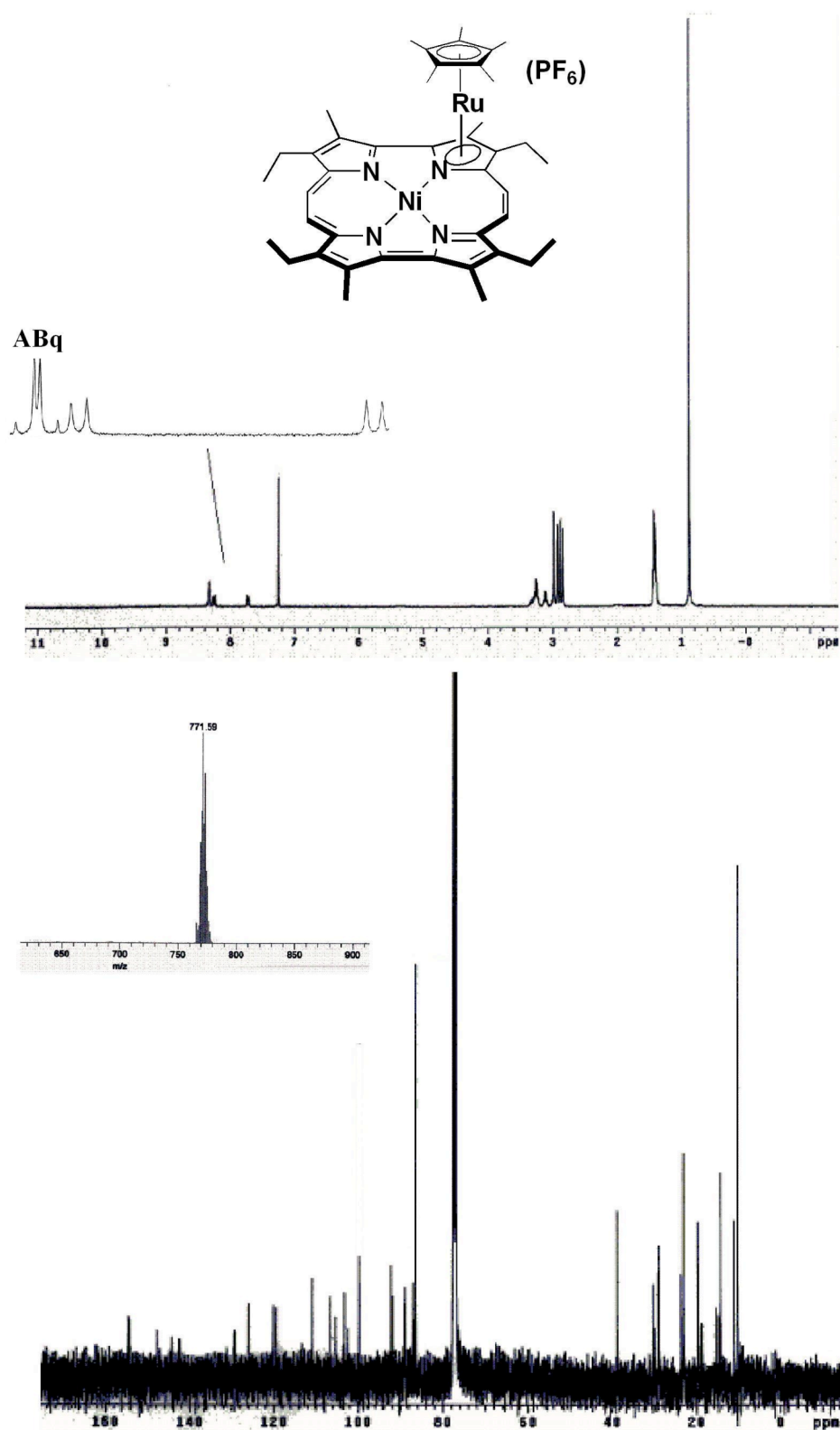


Figure S10. ¹H and ¹³C NMR in CDCl₃ and Mass Spectra for **2a**.

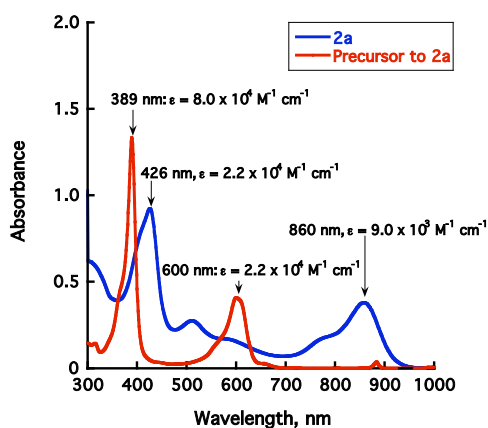


Figure S11. UV-vis spectra of **2a** and its ruthenium-free precursor, (EtioPc)Ni recorded in CH_2Cl_2 .

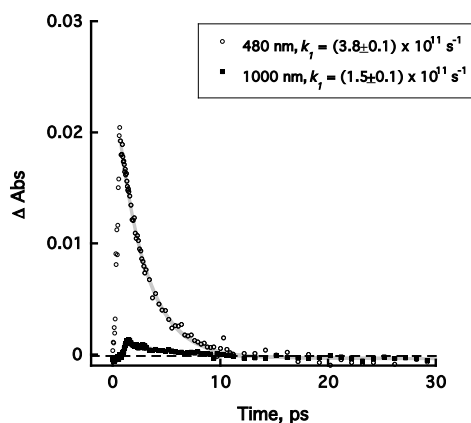


Figure S12. Decay time profile of the absorbance feature at 480 and at 1000 nm of **2a** in CH_2Cl_2 (Corresponds to fs lfp shown in Figure 12b of article text). Both were best fit to a single exponential.

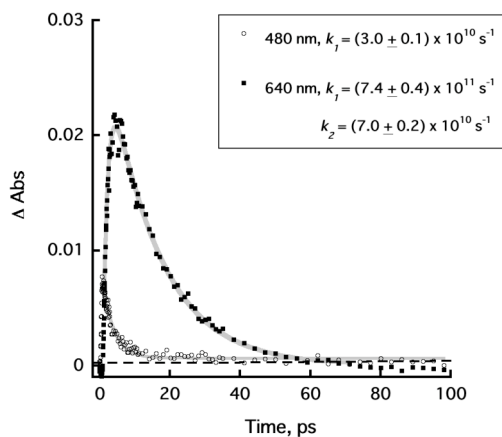


Figure S13. Decay time profile of the absorbance feature at 480 (single exponential) and at 640 nm (double exponential) for the ruthenium-free precursor to **2a** in CH_2Cl_2 (Corresponds to fs lfp shown in Figure 12a of article text).

Compound 2b:

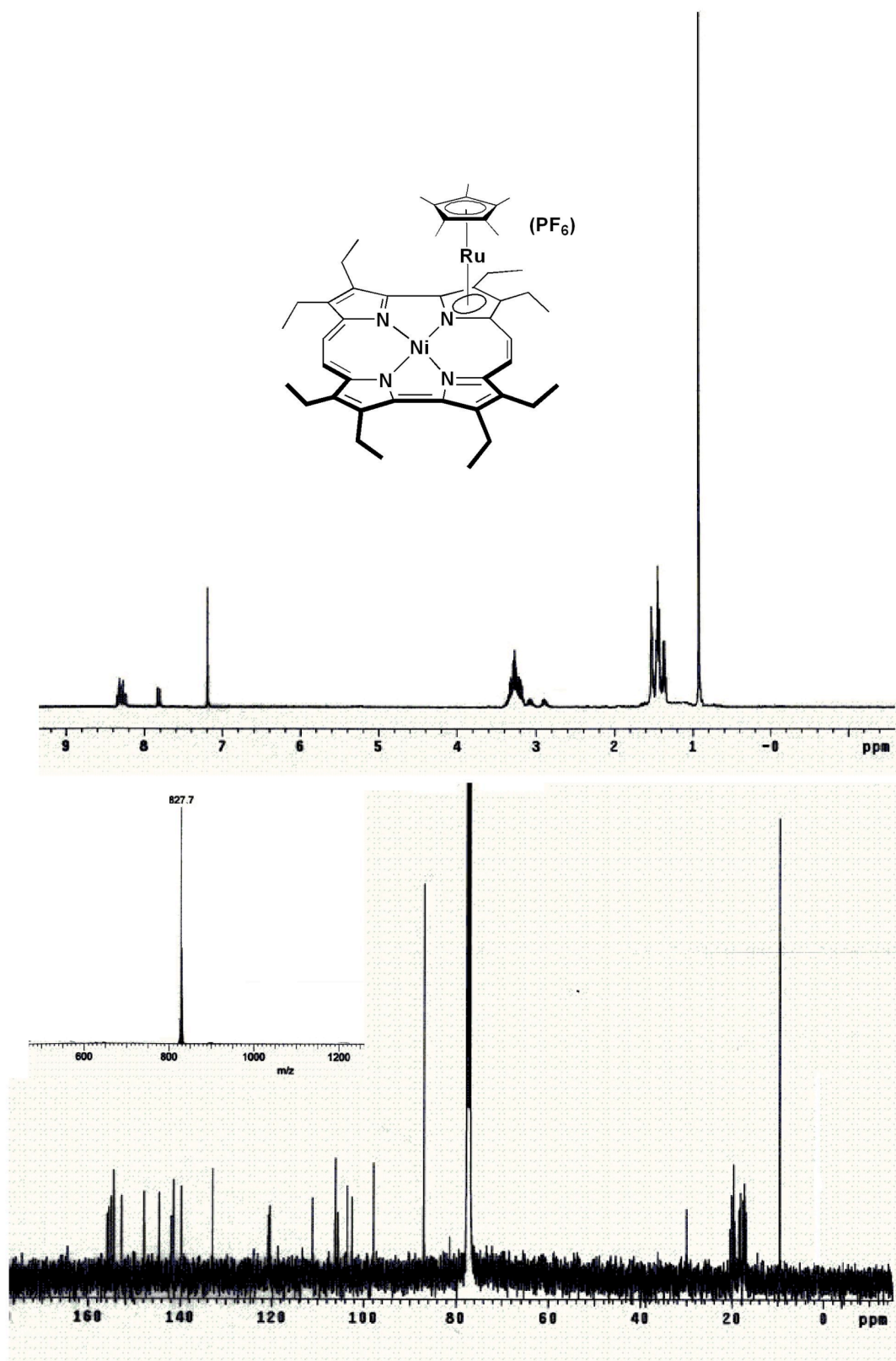


Figure S14. ¹H and ¹³C NMR in CDCl₃ and Mass Spectra for **2b**.

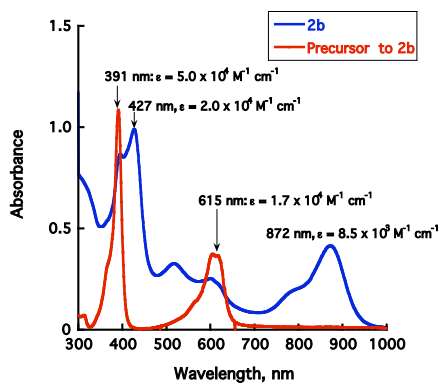


Figure S15. UV-vis spectra of **2b** and its ruthenium-free precursor (OEPc)Ni recorded in CH_2Cl_2 .

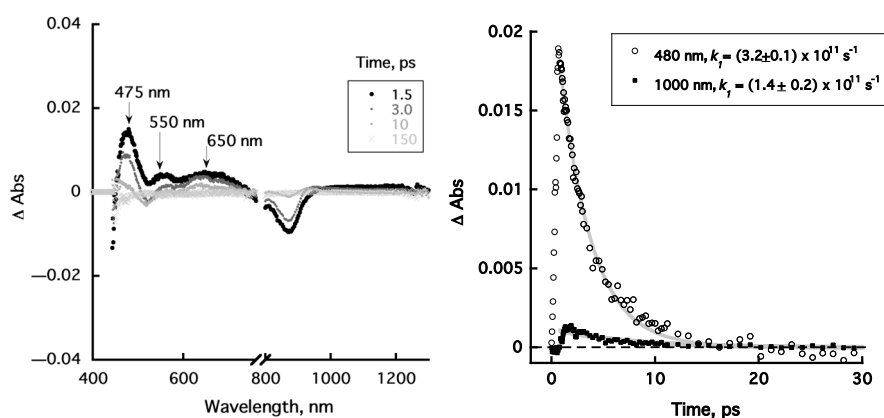


Figure S16. a) Transient absorption spectra of **2b** in CH_2Cl_2 taken at the indicated times after femtosecond laser pulse irradiation by a 420 nm laser at 298 K. b) Decay time profile of the absorbance feature at 480 and at 1000 nm. Both were best fit to a single exponential.

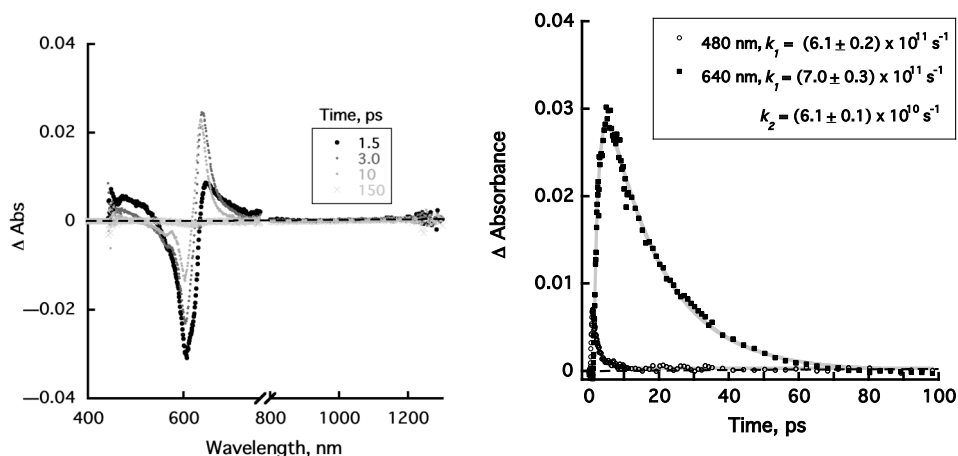


Figure S17. a) Transient absorption spectra of the ruthenium-free precursor to **2b**, (OEPc)Ni in CH_2Cl_2 taken at the indicated times after femtosecond laser pulse irradiation by a 390 nm laser at 298 K. b) Decay time profile of the absorbance feature at 480 nm (single exponential) and at 640 nm (double exponential decay).

Compound 2c:

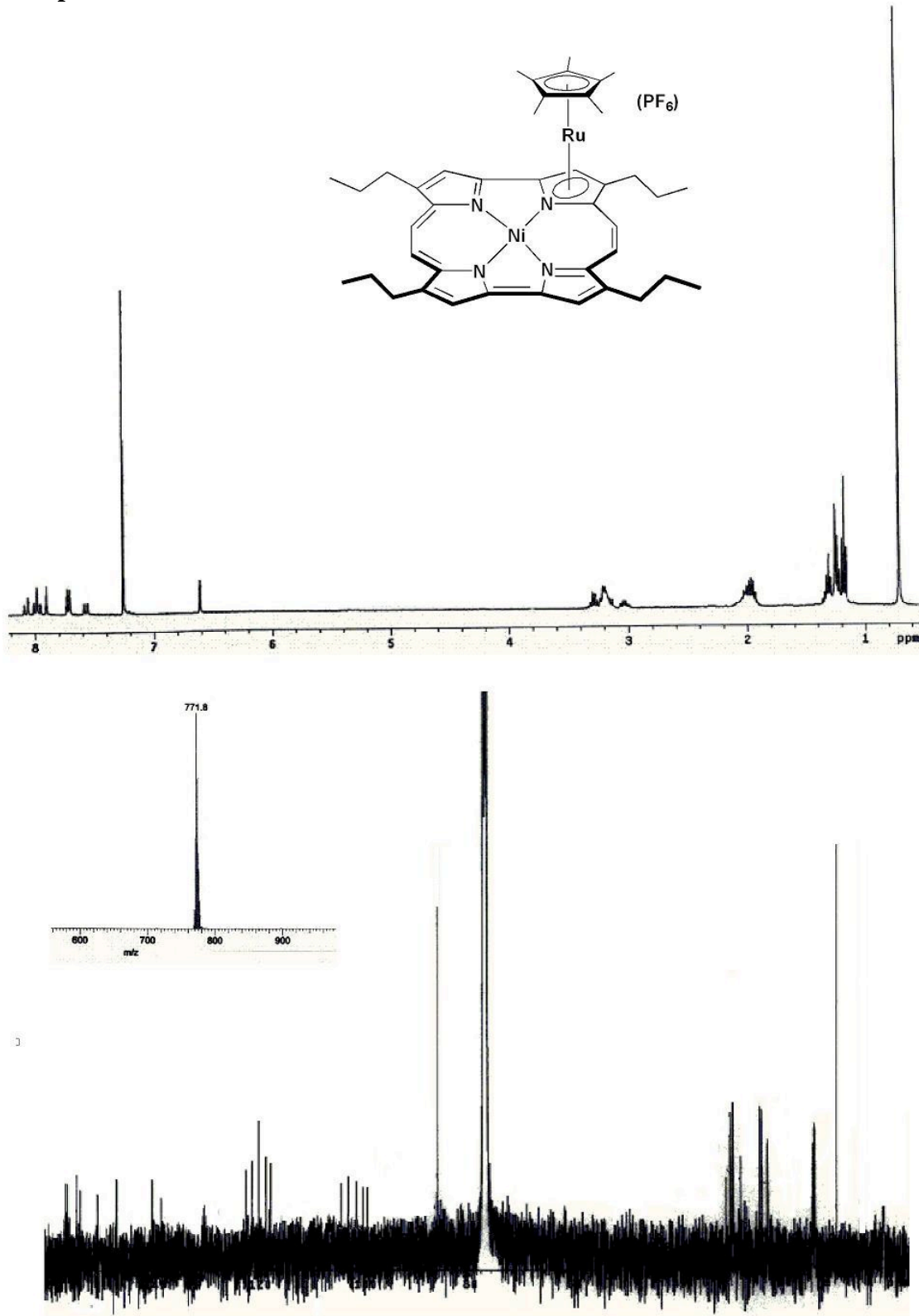


Figure S18. ¹H and ¹³C NMR in CDCl₃ and Mass Spectra for **2c**.

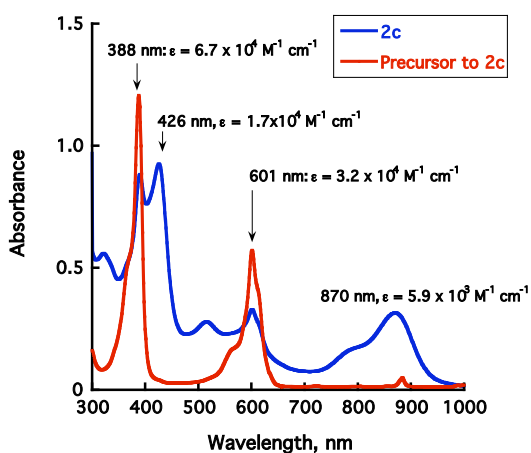


Figure S19. UV-vis spectra of **2c** and its ruthenium-free precursor, (TPrPc)Ni recorded in CH_2Cl_2 .

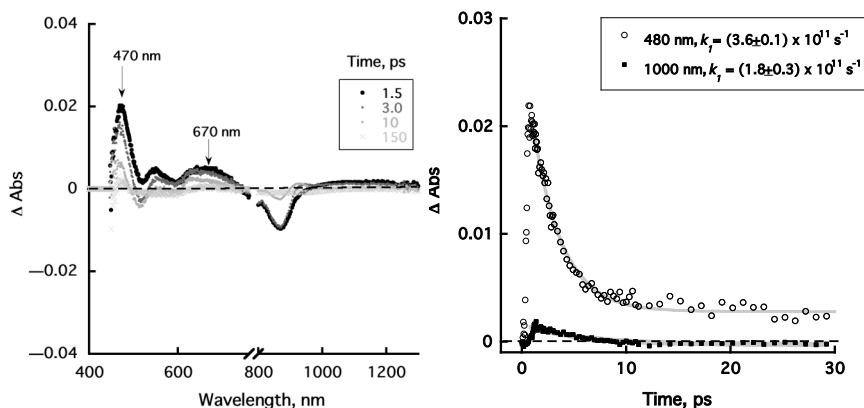


Figure S20. a) Transient absorption spectra of **2c** in CH_2Cl_2 taken at the indicated times after femtosecond laser pulse irradiation by a 420 nm laser at 298 K. b) Decay time profile of the absorbance feature at 480 and at 1000 nm. Both were fit to a single exponential.

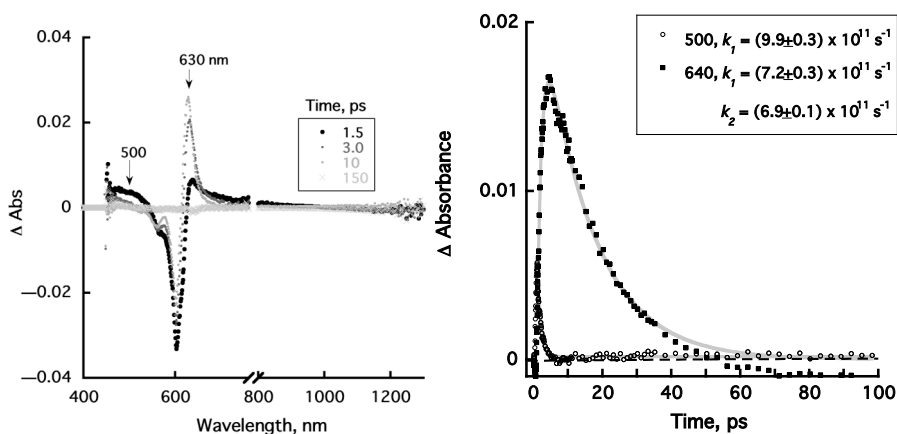


Figure S21. a) Transient absorption spectra of the ruthenium-free precursor to **2c**, (TPrPc)Ni in CH_2Cl_2 taken at the indicated times after femtosecond laser pulse irradiation by a 390 nm laser at 298 K. b) Decay time profile of the absorbance feature at 480 nm (single exponential) and at 640 nm (double exponential decay).

Compound 3a:

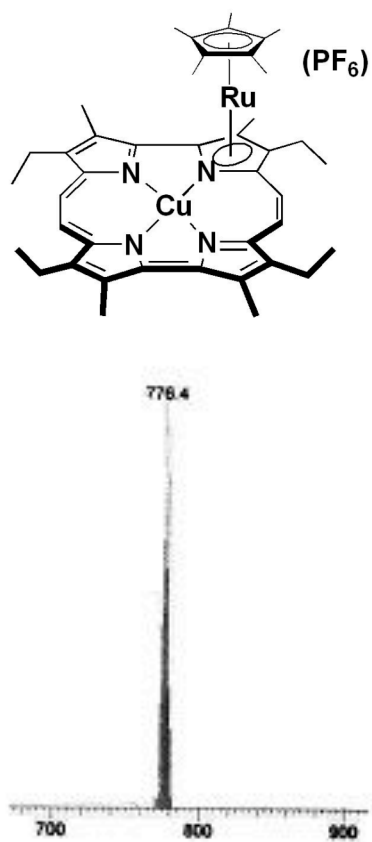


Figure S22. Mass Spectrum of **3a**.

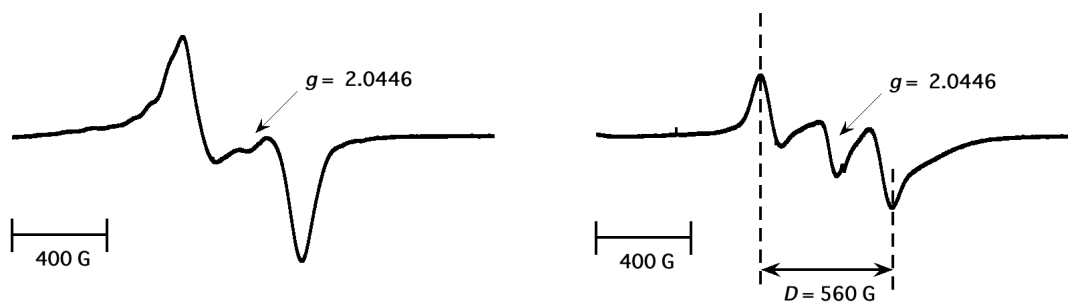


Figure S23. ESR taken in CH_2Cl_2 at 4 K (a) **3a**, $[(Etiopc)Cu(RuCp^*)](PF_6)$ (b) **3a**, $[(Etiopc)Cu(RuCp^*)](PF_6)$ after treating with one equiv. of $Ru(bpy)_3^{3+}$

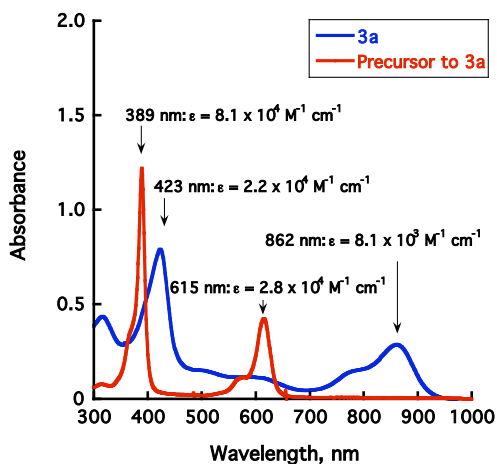


Figure S24. UV-vis spectra of **3a** and the ruthenium-free precursor to **3a**, (EtiO)Cu recorded in CH_2Cl_2 .

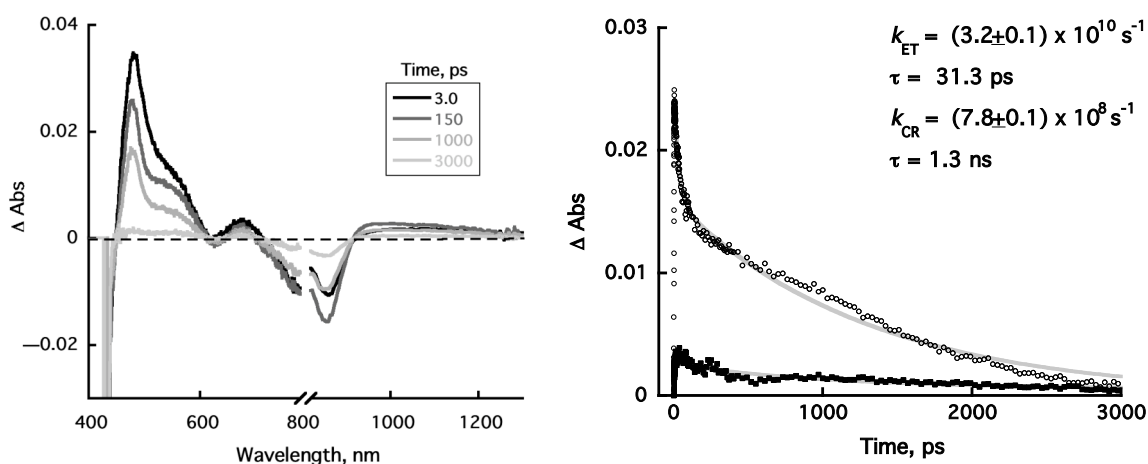


Figure S25. a) Transient absorption spectra of **3a** in CH_2Cl_2 taken at the indicated times after femtosecond laser pulse irradiation by a 420 nm laser at 298 K. b) Decay time profile of the absorbance feature at 500 nm (□) and at 1100 nm (■). Rates were determined by fit of a double exponential to the time profile at 500 nm.

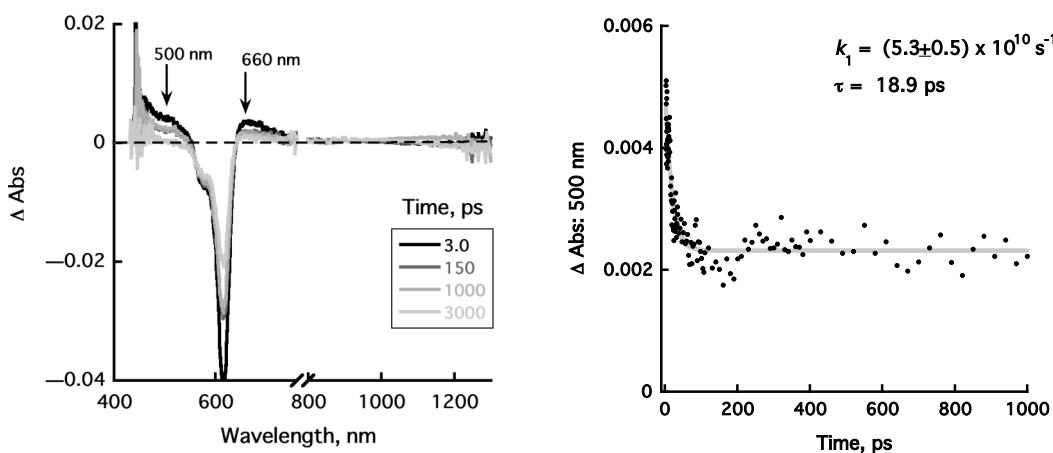


Figure S26. Transient absorption spectra of the ruthenium-free precursor to **3a**, (EtiO)Cu in CH_2Cl_2 taken at the indicated times after femtosecond laser pulse irradiation by a 390 nm laser at 298

Compound 3b:

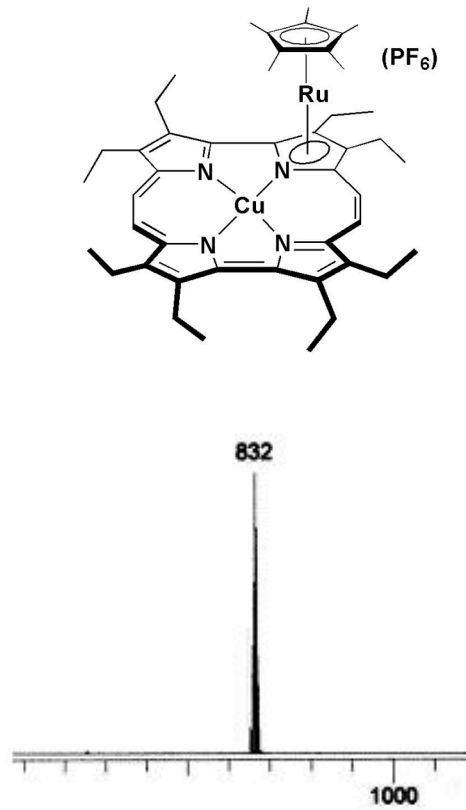


Figure S27. Mass Spectrum for **3b**.

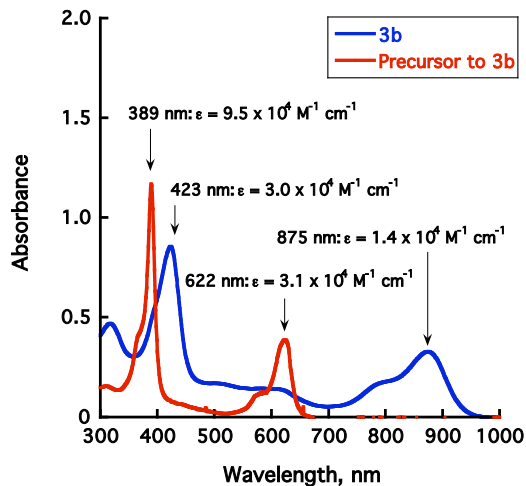


Figure S28. UV-vis spectra of **3b**, and the ruthenium-free precursor to **3b**, (OEPc)Cu recorded in CH_2Cl_2 .

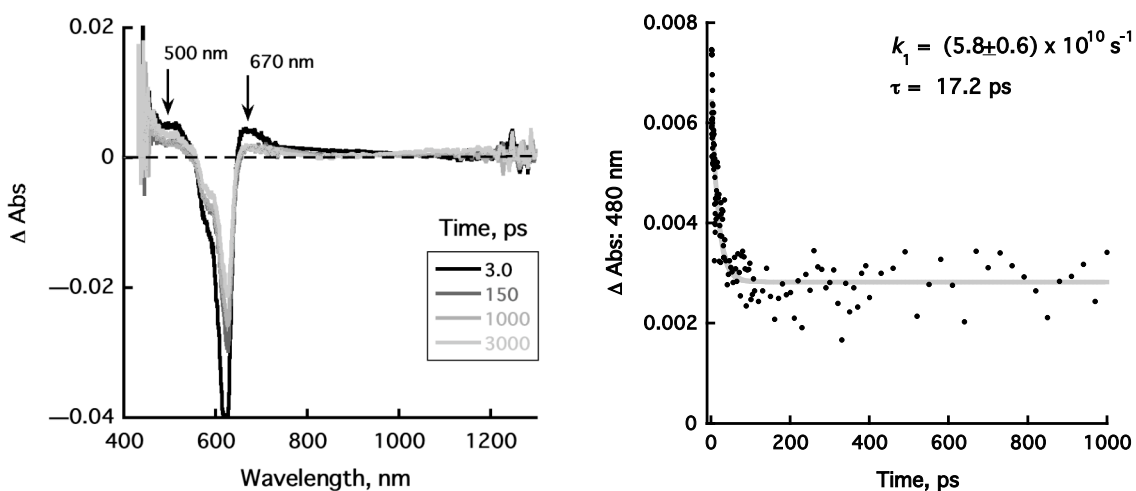


Figure S29. Transient absorption spectra of the ruthenium-free precursor to **3b**, (OEPc)Cu in CH_2Cl_2 taken at the indicated times after femtosecond laser pulse irradiation by a 390 nm laser at 298 K

Compound 3c

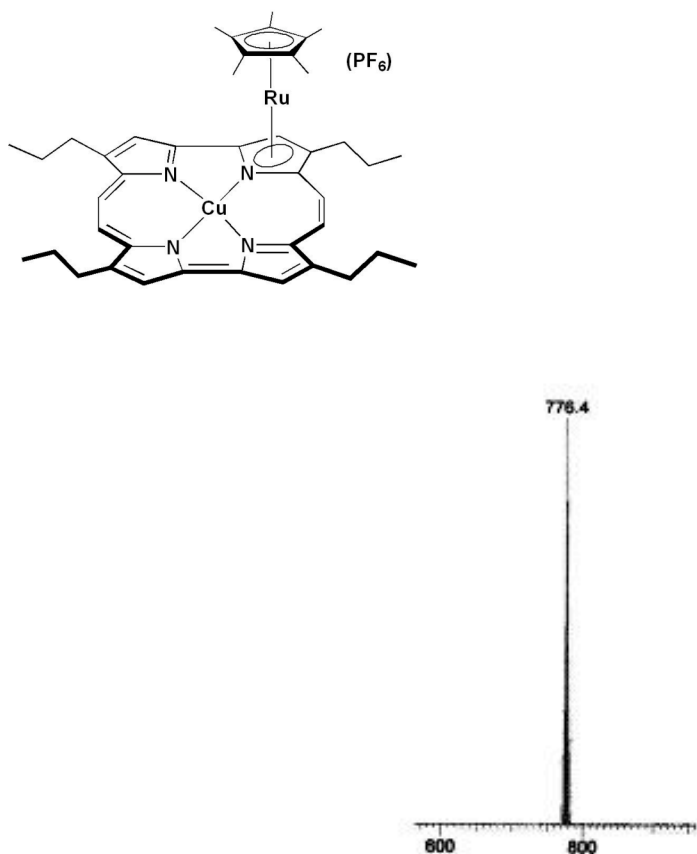


Figure S30. Mass Spectrum for 3c.

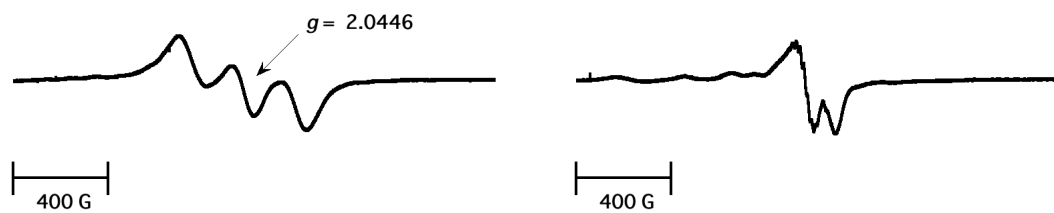


Figure S31. ESR taken in CH₂Cl₂ at 4 K (a) 3c, [(TPrPc)Cu(RuCp*)](PF₆) (b) 3c, [(TPrPc)Cu(RuCp*)](PF₆) after treating with one equiv. of Ru(bpy)₃³⁺

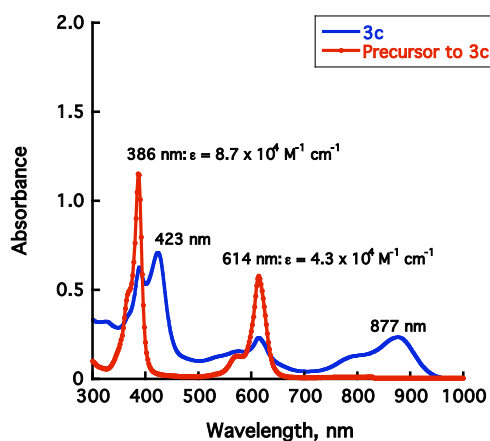


Figure S32. UV-vis spectra of **3c**, and the ruthenium-free precursor to **3c**, (TPrPc)Cu recorded in CH₂Cl₂.

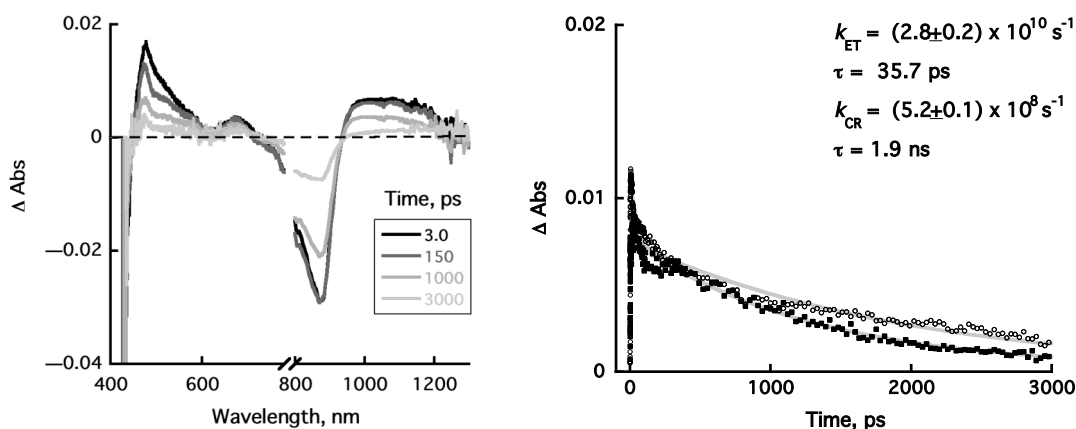


Figure S33. a) Transient absorption spectra of **3c** in CH₂Cl₂ taken at the indicated times after femtosecond laser pulse irradiation by a 420 nm laser at 298 K. b) Decay time profile of the absorbance features at 480 (□)1000 (■) nm.

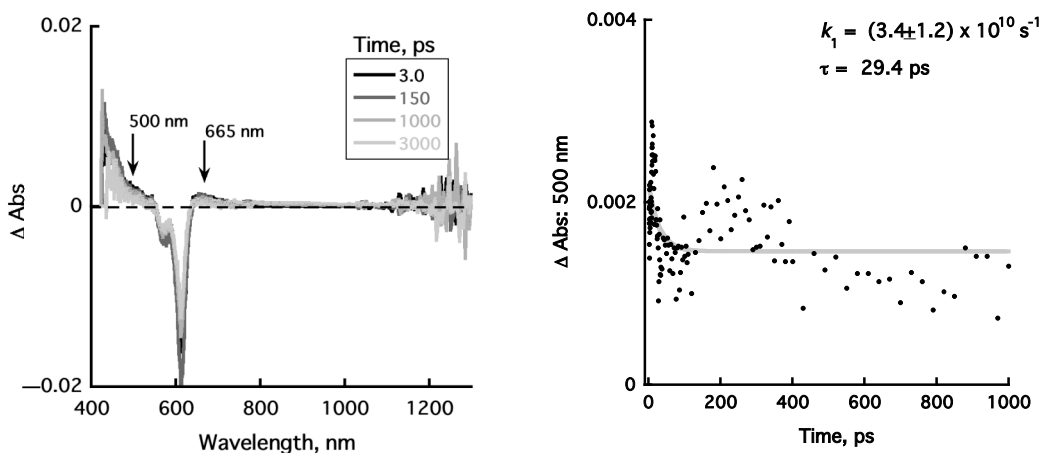


Figure S34. Transient absorption spectra of the ruthenium-free precursor to **3c**, (TPrPc)Cu in CH₂Cl₂ taken at the indicated times after femtosecond laser pulse irradiation by a 390 nm laser at 298 K.

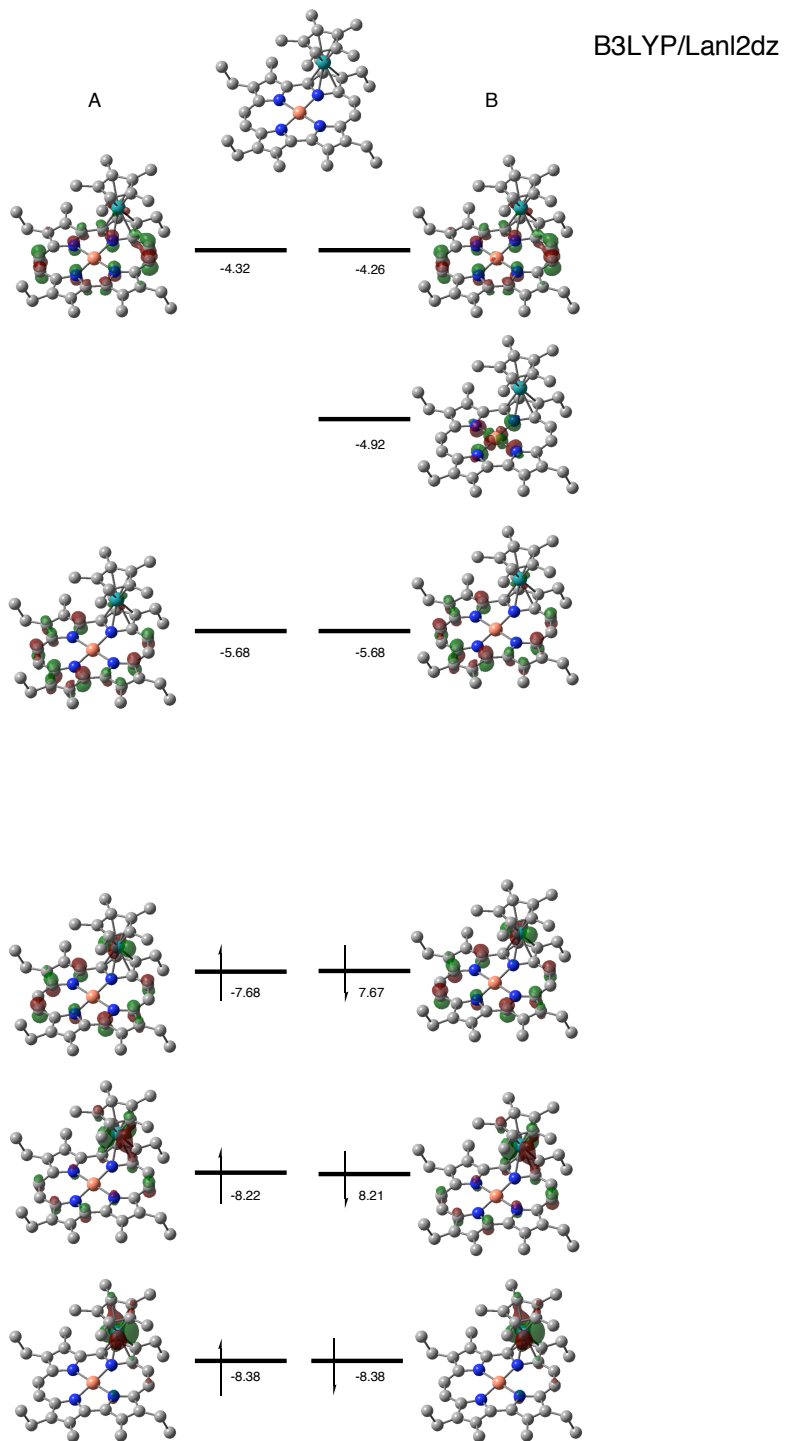


Figure S35. DFT calculations. These results lead to the conclusion that $d_{x^2-y^2}$ is the ground-state orbital. Note: on this basis, we expect the HOMO for the molecule to be the RuCp* (for photo-induced electron transfer to ring). However, these calculations do not account for solvent stabilization in solution, which leads to electron-transfer oxidation occurring at the RuCp* center.

Table S1. Half-wave Potentials (V vs SCE) of Ni and Cu Porphycenes

solvent	metal	macrocycl e	ox			red		ref
			3rd	2nd	1st	1st	2nd	
CH ₂ Cl ₂	Ni ^a	EtioPc	1.71	1.17	0.91, 0.81	-1.08	-1.46	tw
		OEPc	1.73	1.15	0.84	-1.03	-1.45	tw
					1.12	0.81	-1.06	-1.46
		TPrPc	1.78	1.44, 1.34	0.98, 0.86	-0.96	-1.36	tw
				1.34	0.90	-0.99	-1.36	15.9
	Cu ^b	EtioPc		1.16	0.92, 0.76	-1.11	-1.47	tw
		OEPc		1.12	0.76	-1.09	-1.46	tw
		TPrPc		1.28	0.94, 0.81	-1.00	-1.37	tw
					1.18	0.88	-0.97	-1.32
	PhCN	Ni	EtioPc	1.76	1.16	0.82	-1.06	-1.47
OEPc			1.74	1.09	0.81	-1.11	-1.47	15.7
Cu		OEPc		1.10	0.83	-1.05	-1.39	15.5

^aContaining 0.1M TBAP as the supporting electrolyte.

^bContaining 0.1M TBAPF₆ as the supporting electrolyte.

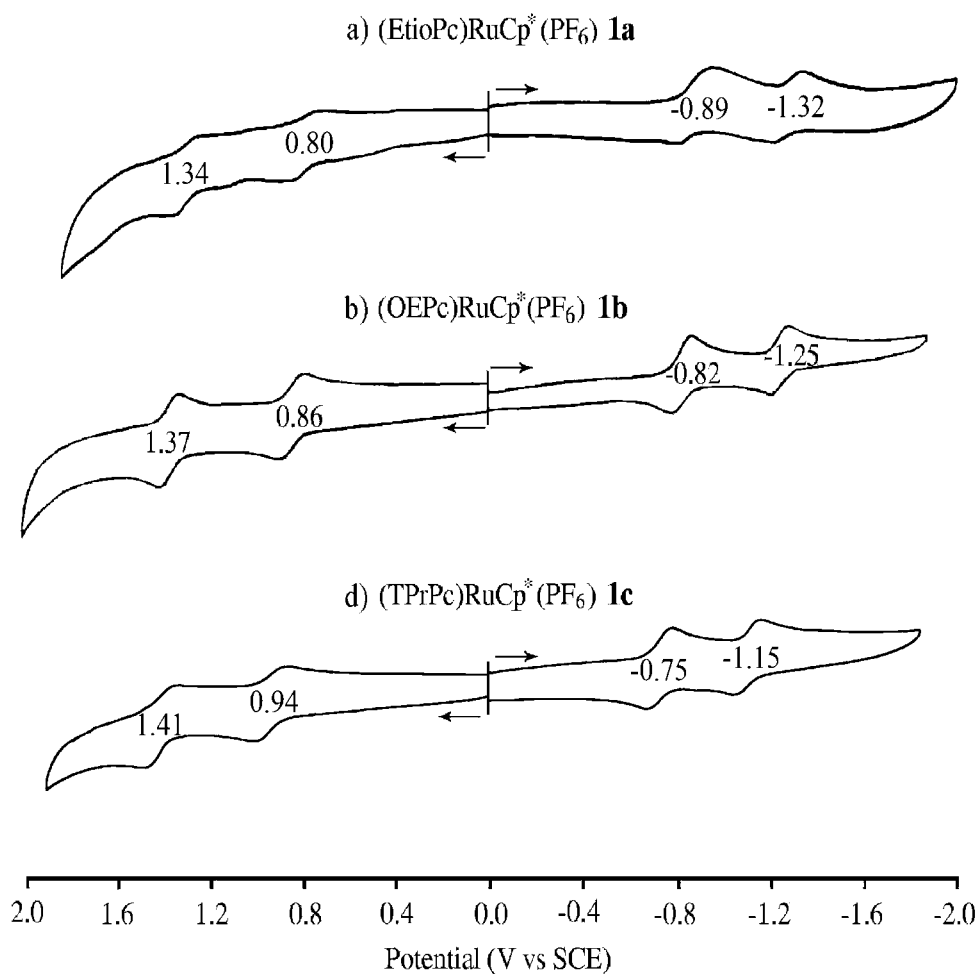


Figure S36. Cyclic voltammograms of (a) (EtioPc)RuCp^{*}(PF₆) (**1a**), (b) (OEPc)RuCp^{*}(PF₆) (**1b**), and (c) (TPrPc)RuCp^{*}(PF₆) (**1c**) under -70°C in CH₂Cl₂ containing 0.1 M TBAPF₆.

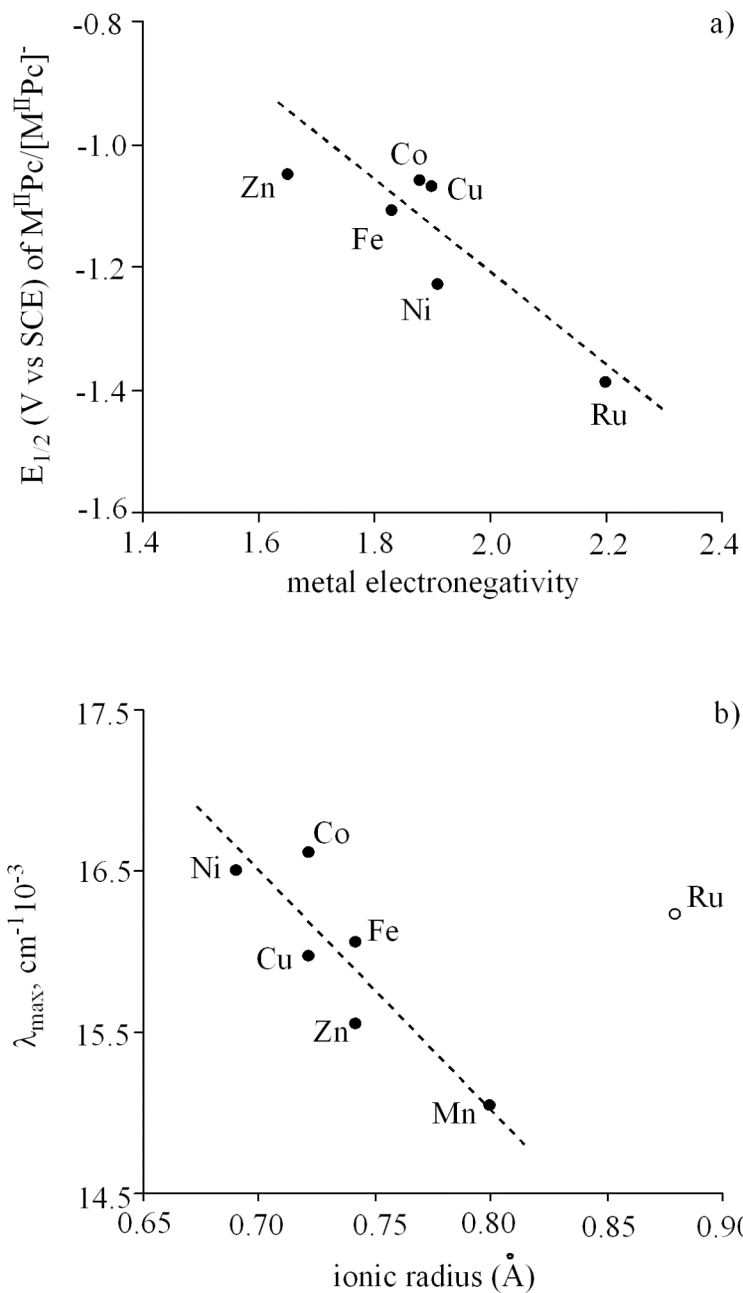


Figure S37. Plot of (a) $E_{1/2}$ (V vs SCE, for $[M^{II}Pc]/[M^{II}Pc]^-$) vs metal electronegativity of porphyrines and (b) the lowest energy transition (λ_{max} , $cm^{-1} \cdot 10^{-3}$) vs radius of central metal ion.

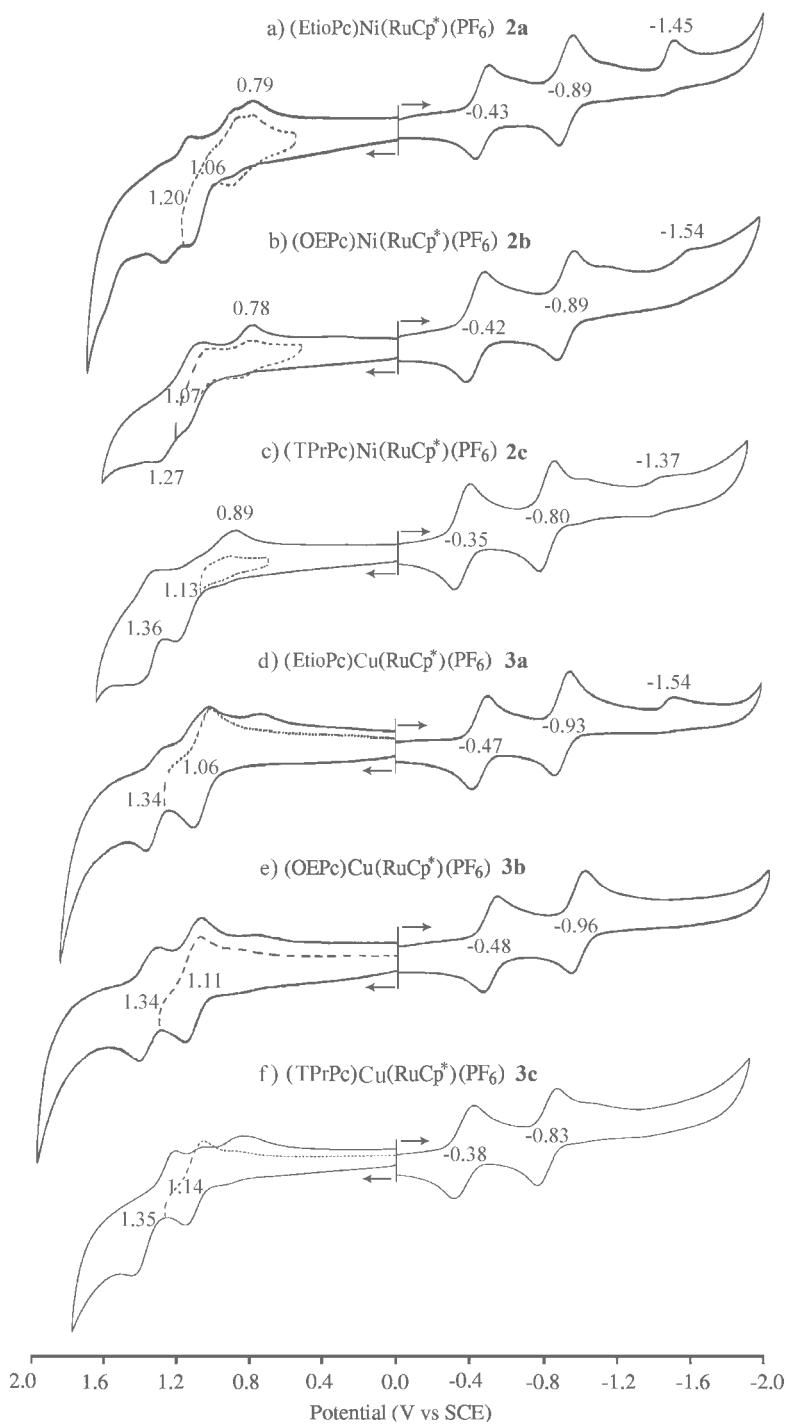


Figure S38. Cyclic voltammograms of complexes **2-3** in CH_2Cl_2 containing 0.1 M TBAPF_6 .

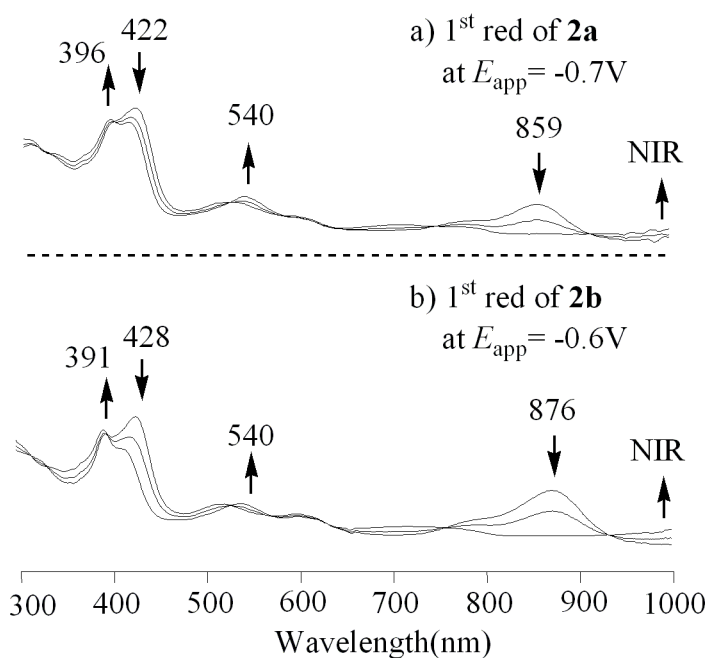


Figure S39. UV-visible spectral changes of **2a** and **2b** during the first reduction in CH_2Cl_2 , 0.1 M TBAPF₆.

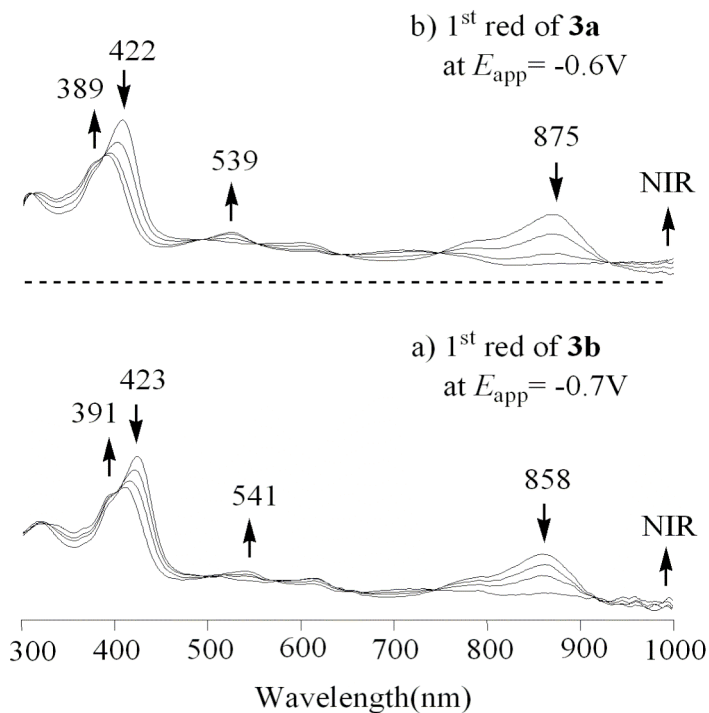


Figure S40. UV-visible spectral changes of **3a**, and **3b** during the first reduction in CH_2Cl_2 , 0.1 M TBAPF₆.

Calculation of the distance between the Two Unpaired Electrons as deduced from the Zero-Field Splitting Constants, the following equation was used:

$$D = \frac{3}{2} \frac{g\mu_B}{r^3}$$

Where, μ_B = Bohr magneton ($= 9.2741 \times 10^{-24} \text{ J T}^{-1}$), r = distance between the two unpaired electrons (in Å), g = g value, and D = zero-field splitting constant (in gauss).

References:

- S1) (a) Vogel, E.; Balci, M.; Pramod, K.; Koch, P.; Hou, X. -L.; Lex, J.; Lausmann, M.; Kisters, M.; Aukauloo, M.A.; Richard, P.; Guillard, R. *Angew. Chem., Int. Ed. Engl.* **1993**, *32*, 1600-1604. (b) Vogel, E.; Koch, P.; Lex, J.; Ermer, O. *Angew. Chem., Int. Ed. Engl.* **1987**, *26*, 928-931. (c) Guillard, R.; Aukauloo, M. A.; Tardieux, C.; Vogel, E. *Synthesis* **1995**, 1480-1482.
- S2) See 9d, and Renner, M. W.; Forman, A.; Wu, W.; Chang, C. K.; Fajer, J. *J. Am. Chem. Soc.* **1989**, *111*, 8618-8621.
- S3) Lin, X. Q.; Kadish, K. M. *Anal. Chem.* **1986**, *57*, 1498-1501.
- S4) (a) Otwinowski, Z.; Minor, W. *Methods in Enzymology*, **1997**, *276*, 307-326 (b) *Macromolecular Crystallography*, Carter C. W. Jr.; Sweets, R. M. Eds.; Academic Press: San Diego, 1997, Part A, 307-326.
- S5) Program for crystal structure solution. Altomare, A.; Burla, M. C.; Camalli, M.; Cascarano, G. L.; Giacovazzo, C.; Guagliardi, A.; Moliterni, A. G. G.; Polidori, G.; Spagna, R. *J. Appl. Cryst.* **1999**, *32*, 115-119.

- S6) Program for the Refinement of Crystal Structures. Sheldrick, G. M. University of Gottingen, Germany, 1994.
- S7) Cooper, R. I.; Gould, R. O.; Parsons, S.; Watkin, D. J. *J. Appl. Cryst.* **2002**, *35*, 168-174.
- S8) Farrugia, L. J. *J. Appl. Cryst.* **1999**, *32*, 837-838.